Impact of the temperature-cloud phase relationship on the simulated Arctic warming during the last interglacial

Nozomi Arima★[1], Masakazu Yoshimori★[1], Ayako Abe-Ouchi[1], Ryouta O'ishi[1], Wing-Le Chan[1], Sam Sherriff-Tadano[2], and Tomoo Ogura[3]

[1]Atmosphere and Ocean Research Institute, The University of Tokyo, Kashiwa, Japan
[2]University of the Ryukyus, Okinawa, Japan
[3]National Institute for Environmental Studies, Tsukuba, Japan
★These authors are joint first authors.

Correspondence to: Masakazu Yoshimori (masakazu@aori.u-tokyo.ac.jp)

Abstract. The Arctic during the last interglacial period (LIG) was considered warmer than it is today. The previous study points to a large difference in the degree of simulated annual-mean Arctic warming among models. While recent reconstructions suggest the disappearance of summer sea ice in the Arctic at the LIG, many climate models fail to capture this feature. It is thus essential to investigate sources of uncertainty in climate models. The current study examines the impact of the temperature-cloud phase relationship. Sensitivity studies are conducted for the first time to explore the potential importance of this relationship in simulating the LIG climate. Two different cloud parameter sets are used for an atmosphere-ocean general circulation model with and without the dynamic vegetation feedback. The model with cloud parametrization that permits liquid water at lower temperatures and a larger fraction of supercooled liquid water at the same temperature simulates a warmer preindustrial (PI) climate, greater annual-mean Arctic warming at the LIG, and substantially reduced summer sea ice cover at the LIG. It is demonstrated that the low-level clouds play a crucial role in controlling the Arctic response via the greenhouse effect. The result indicates the importance of the temperature-cloud phase relationship in simulating the Arctic climate at the LIG. It also highlights the importance of accurately simulating modern sea ice thickness and representing the processes that affect the fraction of supercooled liquid water in clouds.

1 Introduction

The Last Interglacial (LIG) refers to the period from 129,000 to 116,000 years ago (Gulev et al., 2021), when the Earth was relatively warm, and ice sheets over the North American and Eurasian continents were relatively small during the Pleistocene glacial cycles (e.g., Cline et al., 2017; McKay et al., 2011; Past Interglacials Working Group of PAGES, 2016; Turney et al., 2020). The global mean temperature is estimated to be about 0.5 to 1.5℃ higher than the Preindustrial (PI) (Gulev et al., 2021). The primary source of external forcing at LIG is the Earth's orbital configuration, in which the Northern Hemisphere (NH) summer solstice is closer to the perihelion under a larger eccentricity, and the Earth's axial tilt is larger by about 0.6º than PI (Otto-Bliesner et al., 2017). However, it is not fully understood how the seasonal and latitudinal

redistribution of insolation causes a warmer climate than today. Indeed, on average, multi-model climate simulations for 127 kaBP yield a negligible difference (-0.02°C) in global annual mean temperature from the PI (Otto-Bliesner et al., 2021).

The Arctic summer at LIG was estimated to be warmer than PI by as much as 4-5°C (Bennike et al., 2001; CAPE, 2006), and has drawn considerable attention, given that the Arctic is currently warming much faster than the rest of the world, and sea ice is decreasing dramatically (e.g., Rantanen et al., 2022; Box et al., 2024). Kageyama et al. (2021) found a positive correlation in summer sea ice area across climate models between equilibrium LIG and transient CO_2 increasing experiments, suggesting that the Arctic warming at LIG is potentially a practical constraint for future projections. While climate models generally simulate summer land warming reasonably well, they tend to underestimate the annual mean Arctic warming compared to what proxy records suggest (Otto-Bliesner et al., 2021). In addition, there is a considerable model spread in the Arctic temperature anomaly from the PI (Otto-Bliesner et al., 2021).

The first comprehensive model-data comparison for the Arctic sea-ice cover was conducted by Kageyama et al. (2021). Recently, Vermassen et al. (2023) examined the presence or absence of sea ice, including in the Central Arctic, based on microfossil assemblages, and argued that the Arctic was essentially ice-free in summer at LIG. While the proxy reconstruction is subject to substantial dating uncertainty and may not necessarily represent LIG conditions (Razmjooei et al., 2024), isotope-enabled modelling studies support a summer-ice-free Arctic: the higher oxygen isotope ratio in Greenland ice cores at LIG is well explained by the absence of sea ice and warmer summer sea-surface temperatures in the Arctic (Malmierca-Vallet et al., 2018). Additional support for the nearly ice-free summer Arctic at LIG is provided by Sime et al. (2023), who applied the emergent relationship between summer temperature increases and sea ice area reductions across models to a reconstructed LIG warming. Nevertheless, only one of the 12 models analyzed by Kageyama et al. (2021) simulated climatologically (long-term mean) ice-free conditions, and a few models occasionally produced ice-free summers (Sime et al., 2023, Figure 4; Sime et al., 2025, Figure 2). O'ishi et al. (2021) reported that dynamic vegetation feedback, in which vegetation type changes in response to local climate change, helps simulate the substantially warmer Arctic at LIG. However, it does not remove summer Arctic sea ice entirely. Guarino et al. (2020) and Diamond et al. (2021) reported that the explicit representation of melt ponds and the consequent improvement of the surface albedo feedback process, leading to better present-day sea ice simulations, play an essential role in 'successfully' simulating the ice-free Arctic summer. Although it may not be fundamental, we note that their model exhibits relatively high climate sensitivity, and the other model with an explicit melt pond representation does not capture the climatologically ice-free condition.

Another potential source of uncertainty in the LIG simulation, which we focus on in this study, is the temperature-cloud phase relationship in models. Here, the cloud phase refers to the state of cloud particles, either cloud droplets (liquid water) or ice crystals (solid water). It is well known that mixed-phase clouds, composed of both liquid and solid cloud particles, are common in the Arctic (Kay et al., 2016; Morrison et al., 2011), and the cloud phase is one of the essential key parameters influencing climate change (Tan et al., 2016; Tsushima et al., 2006; Yoshimori et al., 2009; Zelinka et al., 2020).

There are two primary effects of phase changes of cloud particles on cloud properties: albedo and lifetime. A warming increases the fraction of supercooled liquid water (SLF) at the expense of ice crystals, provided that the total amount of

water is constant. Because cloud droplets are generally smaller than ice crystals and are more numerous, an increase in SLF induces surface cooling via increased cloud albedo (Murray et al., 2021). Cloud droplets require more time to grow and precipitate than ice crystals because of their smaller size, resulting in a slower autoconversion rate. In addition, the saturation vapor pressure is higher against the liquid water surface than the ice surface, and ice crystals tend to grow faster at the expense of cloud droplets (the so-called Wegener–Bergeron–Findeisen process). Therefore, an increase in SLF leads to a longer cloud residence time and a greater cloud amount over a given time interval. The more clouds there are, the less shortwave (SW) radiation reaches the surface (cooling), while more longwave (LW) radiation is emitted back to the surface (warming). One important conclusion from this reasoning is that the warming effect should dominate in Arctic winter when insolation is very limited (Tan and Storelvmo, 2019) and Arctic warming is seasonally large (e.g., Screen and Simmonds, 2010). In contrast to the previous work by Kageyama et al. (2021), which emphasized the importance of shortwave (SW) radiative feedback, we highlight LW radiative feedback as an active player. The representation of the cloud-phase change process may be important for simulating the Arctic climate at LIG, although the same reasoning applies to other interglacial periods. Furthermore, it is essential to note that the temperature-cloud phase relationship is extremely diverse among models (McCoy et al., 2015), and even in the recent CMIP6 models (Tan et al., 2025). Whereas it is the first time that the impact of cloud phase representation is investigated for the LIG simulation, the effect has been examined in the context of climate sensitivity (Tan et al., 2016), glacial inception (Sagoo et al., 2021), and Atlantic overturning circulation at the Last Glacial Maximum (Sherriff-Tadano et al., 2023) in previous studies. A broader review of this topic, as well as Arctic amplification, is provided by Yoshimori et al. (2025) and the references therein.

The primary purpose of this study is to evaluate the effect of cloud-phase temperature dependency on LIG Arctic simulations. We are particularly motivated to investigate surface air temperature and sea ice because previous studies show substantial multi-model spread and discrepancies with proxy reconstructions in both fields (Otto-Bliesner et al., 2021; Kageyama et al., 2021). For simplicity, this study assumes a fixed relationship between temperature and cloud phase across climates, whereas in reality, this relationship varies with aerosol distribution. It examines the sensitivity of simulated LIG climate to the specified temperature-phase relation. Additionally, we discuss whether the magnitude of this effect is comparable to the range of multi-model spreads in LIG simulations. By doing so, we aim to determine whether this effect warrants concern in the LIG climate simulation.

2 Models and cloud parameters

2.1 Models

This study employs two climate models: an atmosphere-ocean general circulation model (AOGCM) with and without a dynamic vegetation component, referred to as MIROC4mV and MIROC4m, respectively. The dynamic vegetation here means the vegetation type is computed in the model based on simulated climate, incorporating the interaction between climate and the geographic distribution of vegetation. We begin with a brief description of MIROC4m. MIROC4m is an

AOGCM that consists of the atmosphere, ocean-sea ice, and land surface components interacting with each other through exchanges of energy, water, and momentum (K-1 model developers, 2004). The atmospheric model component is based on the primitive equations and has a horizontal resolution limited by the T42 spectral truncation (~2.8°×2.8°), with 20 vertical levels. The land surface component has the same horizontal resolution as the atmospheric component, with one canopy layer, five soil layers, and a maximum of three snow layers. The ocean model component is based on the primitive equations under the Boussinesq approximation. It has a horizontal resolution of 1.4° in longitude and varies from 0.56° to 1.4° in latitude (with higher resolution toward the equator), comprising 43 vertical levels. The sea ice model component, which computes thermodynamic and dynamic processes, uses the same horizontal resolution as the oceanic component. Fourier filtering is applied to the ocean grids at NH high latitudes to reduce computational cost, as the zonal grid spacing converges toward the North Pole. We note that this filter smooths the large-scale zonal feature in sea ice variables. This climate model runs computationally efficiently and has been used in many paleoclimate studies (e.g., Chan and Abe-Ouchi, 2020; Kuniyoshi et al., 2022; Sherriff-Tadano et al., 2023). As stated in the Introduction, Sherriff-Tadano et al. (2023) is particularly relevant, as they demonstrated the importance of cloud parameterization in the LGM climate, which is employed in the current study.

MIROC4mV is a model that couples MIROC4m with the dynamic vegetation component (LPJ-DGVM) (O'ishi et al., 2009; Sitch et al., 2003). Dominant vegetation is represented by the plant functional type and is determined annually for each grid cell based on monthly temperature, precipitation, and sunlight, averaged over the most recent 20 years. The prescribed atmospheric CO_2 concentration also affects plants through fertilization. These variables are passed from the atmospheric component to the LPJ-DGVM, and the diagnosed vegetation type is then passed to the land surface component. By doing so, it is possible to simulate the interaction between climate and vegetation changes. This vegetation-coupled climate model has also been used in previous studies. As stated in the Introduction, O'ishi et al. (2021) are particularly relevant, as they demonstrated the importance of vegetation feedback for LIG Arctic warming, and Hirose et al. (2025) are relevant, as they identified remnant glacial ice sheets as a critical factor in the diversity of past interglacials.

2.2 Two cloud parameter sets

We examine differences in the climate response to external forcing using two cloud parameter sets, "S" and "L", introduced by Sherriff-Tadano et al. (2023) as models "A" and "C," respectively. As defined below, "S" is named after more solid water and "L" after more liquid water at the same temperature. Three parameter values are different between the two sets: a) the lowest temperature (T_{ice} in Eq. 1) at which supercooled liquid water droplets can exist; b) a coefficient of autoconversion rate for rain (α in Eq. 2); and c) a coefficient of ice sedimentation rate (V_0 in Eq. 3). Note that the actual values are summarized in Table 1.

Table 1: Perturbed cloud parameter values

Cloud parameter set	T_{ice} (°C)	α	V_0
S	-15	0.010	0.25
L	-28	0.025	0.30

In MIROC4m, SLF, taking the range from 0 to 1, is parameterized in such a way that all cloud particles are solid below T_{ice} and liquid above 0°C, and SLF is linearly interpolated in-between (Ogura et al., 2008):

$$SLF(T) = \begin{cases} 0 & (T \le T_{ice}) \\ (T - T_{ice})/(0 - T_{ice}) & (T_{ice} < T < 0) \\ 1 & (0 \le T) \end{cases} \quad (1)$$

where the unit for T and T_{ice} is in °C. The difference between cloud parameter sets S and L in SLF exists for the range between -28 and 0°C, and it is always larger in L, meaning that more cloud liquid water exists in L with a given amount of total cloud water (Fig. 1). The original setting of the model follows the temperature dependency of cloud phase in S. Still, L is designed to be closer to the empirical relationship between temperature and cloud phase, obtained from recent satellite-based observations (Fig. 4 in Sherriff-Tadano et al., 2023).

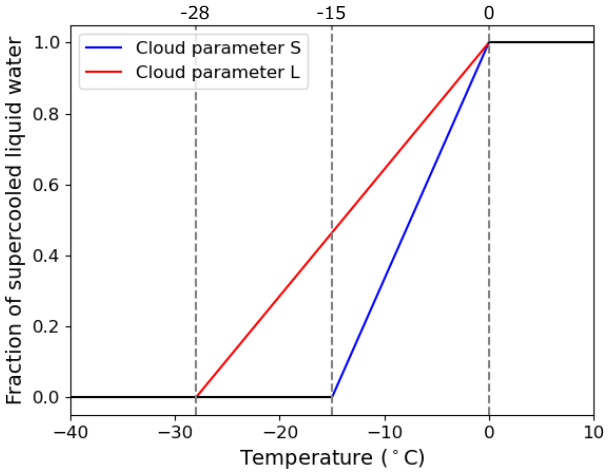

Figure 1: Fraction of supercooled liquid water in the two cloud-parameter sets S ($T_{ice} = -15$°C) and L ($T_{ice} = -28$°C). Vertical gray dashed lines indicate the temperature ranges within which solid and liquid phases coexist in cloud particles.

A complication arises in the coupled-model sensitivity experiments because a single-parameter perturbation disturbs the global energy balance of the Earth, leading the model to drift away from the realistic modern climate. To avoid this issue, Sherriff-Tadano et al. (2023) also adjusted the two other cloud parameter values. Rain rate P_{rain} is parameterized as

$$P_{rain} = -\frac{\partial l_L}{\partial t} = \frac{\alpha \rho l_L^2}{\beta + \gamma \frac{N_c}{\rho l_L}} + C_c F_p l_L, \quad (2)$$

where l_L is the cloud liquid water content, ρ is the air density, N_c is the cloud droplet number concentration, F_p is the precipitation flux from the layer above, α, β, γ and C_c are constants (Ogura et al., 2008). In the cloud parameter set L, the coefficients associated with autoconversion rate α in Eq. (2) is increased compared to set S (Table 1). Ice sedimentation rate P_{ice} is parameterized as

$$P_{ice} = -\frac{\partial l_F}{\partial t} = \left\{\frac{V_0(\rho l_F)^{\delta}}{\Delta z}\right\} l_F. \quad (3)$$

where l_F is the cloud ice content, Δz is the thickness of the model layer, and V_0 and δ are constants (Ogura et al., 2008). In the cloud parameter set L, the coefficient associated with ice sedimentation rate V_0 in Eq. (3) is increased compared to set S (Table 1). The increase in both α and V_0 generally reduces cloud amount.

We verified that the cloud liquid water has a longer mean lifetime than cloud ice water in the model (Fig. S1), which is qualitatively consistent with the discussion in the Introduction. Therefore, an increase in SLF is expected to result in a larger cloud amount when averaged over a specific period.

3 Experiments

A list of numerical experiments is presented in Table 2 for both MIROC4mV (with a dynamic vegetation component) and MIROC4m (without a dynamic vegetation component). In this paper, we primarily present the results of MIROC4mV because it is considered more realistic. The results of MIROC4m are added only when deemed necessary in the Discussion (Sect. 5).

Using the MIROC4mV, we conducted equilibrium climate simulations for PI and LIG with cloud parameter sets S and L. First, we performed the PI experiments with an integration period of 3000 years (PIvS and PIvL). Note that the small letter "v" refers to dynamic vegetation, and "S" and "L" refer to the cloud parameter set. Starting from the quasi-equilibrium states of PIvS and PIvL, we conducted the equilibrium LIG experiments following the PMIP4 protocol (Otto-Bliesner et al., 2017) with an integration period of 2000 years (LIGvS and LIGvL).

We also examined the sensitivity of cloud-phase representation using the model without dynamic vegetation, because most models used in previous LIG simulations did not include it. There is concern that differences in simulated LIG climates may lead to varying sensitivities to cloud parameterization. To assess the robustness of the results, we repeated the simulations using MIROC4m (PIfS, PIfL, LIGfS, and LIGfL). The small letter "f" refers to fixed vegetation. Note that this study was not motivated to explore the direct interaction between vegetation and cloud-phase feedback processes. To isolate the effect of dynamic vegetation feedback through a comparison of MIROC4mV and MIROC4m, the dominant (most frequent) vegetation type for each grid cell simulated by PIvS over the last 100 years is prescribed for the corresponding grid cell in both PIfS and LIGfS experiments, and that simulated by PIvL is prescribed in both PIfL and LIGfL experiments. They are described in Sect. 5.1. This approach prevents bias in the simulated modern vegetation from directly influencing the comparison between MIROC4mV and MIROC4m.

180

Table 2: A list of numerical experiments with the MIROC4mV and MIROC4m.

Experient name	Model	Vegetation	Boundary conditions (see Table 3)	Cloud parameter set	Integration length (years)
PIvS	MIROC4mV	Dynamic	PI	S	3000
PIvL	MIROC4mV	Dynamic	PI	L	3000
LIGvS	MIROC4mV	Dynamic	LIG	S	2000
LIGvL	MIROC4mV	Dynamic	LIG	L	2000
PIfS	MIROC4m	Fixed	PI	S	2000
PIfL	MIROC4m	Fixed	PI	L	2000
LIGfS	MIROC4m	Fixed	LIG	S	2000
LIGfL	MIROC4m	Fixed	LIG	L	2000

Table 3: Boundary conditions (LIG follows the PMIP4 protocol described by Otto-Bliesner et al. (2017))

Boundary conditions	Eccentricity	Obliquity (°)	Longitude of perihelion from the autumnal equinox (°)	CO_2 (ppm)	CH_4 (ppb)	N_2O (ppb)
PI	0.016720	23.45	102.04	285.431	863.303	270.266
LIG	0.039378	24.05	275.41	275.000	685.000	255.000

185 This paper expresses the difference between LIG and PI (LIG – PI) as ΔLIG for brevity. For example, the difference between LIG and PI in experiments with the cloud parameter set S in MIROC4mV (LIGvS – PIvS) is expressed as ΔLIGvS, whereas that with the cloud parameter set L is described as ΔLIGvL. The last 100 years of each experiment are used in the following analysis for the coupled climate models of MIROC4mV and MIROC4m.

Additionally, we conducted experiments using the atmospheric component of MIROC4m, an atmospheric GCM, to isolate
190 the impact of three individual parameters in the cloud parameter sets separately. The lower boundary conditions, i.e., sea surface temperature and sea ice, are taken from the coupled models. The details of the experimental design and its results are described in Appendix A.

4 Analysis method

4.1 Calendar adjustments

Since the shape and precession phase of the Earth's orbit around the Sun are different at LIG from PI, the angular velocity, which depends on the Sun-Earth distance, differs between the two experiments for each season. The astronomical season may be defined by the angle from the moving vernal equinox, e.g., 90 degrees for the summer solstice. Applying a modern calendar to both LIG and PI yields a comparison of slightly shifted seasons. To minimize this undesired effect, we used the calendar adjustment introduced by Bartlein and Shafer (2019) for the monthly mean values. This adjustment enables us to more accurately evaluate the seasonal difference between LIG and PI, which is essential for comparing the simulation with proxies whose records are dominated by a specific season. While this adjustment is appropriate for comparing the model and data, differences in month length between the two periods (PI and LIG) may introduce issues in energy budget analysis, which relies on conservation, as noted by Sime et al. (2025). While our energy balance analysis, described in the next section, is applied independently for each month and the interpretation should not be affected by differences in month length, we also examined an alternative calendar definition: the mid-month date is defined according to the fixed-angle calendar, and the month length is fixed for 31 days, with 15 days before and after the mid-month date. The results change little and are presented in the Supplementary Materials. We also note that the calendar adjustments are not applied when calculating the annual mean values.

4.2 Partial surface temperature change

We applied the surface energy balance analysis to quantify the contributions of individual feedback processes to changes in surface temperature (ST), following Lu and Cai (2009). This method converts each energy-flux term in W m^{-2} between the two experiments into a partial ST change in K, whose sum is an excellent approximation to the simulated ST change.

The energy balance equation at the surface may be given by

$$N = (1-a)S^{\downarrow} + F^{\downarrow} - F^{\uparrow} - LE - H \tag{4}$$

where $S^{\downarrow}$ is downward SW radiation with a being the surface albedo, and $F^{\downarrow}$ and $F^{\uparrow}$ are downward and upward LW radiation, respectively. H and LE are sensible and latent heat fluxes (positive upward), respectively, and N is the heat storage rate in the subsurface (e.g., heat uptake by the ocean and heat conduction into the soil layers).

The perturbation equation for the difference between the two experiments, denoted by Δ, is written as

$$\begin{aligned} 4\sigma\bar{T}^3\Delta T \approx \Delta F^{\uparrow} = &-\Delta\alpha\bar{S}^{\downarrow} - \Delta\alpha\Delta S^{\downarrow} + (1-\bar{a})\Delta S^{\downarrow,clr} + \Delta F^{\downarrow,clr} \\ &+(1-\bar{a})\Delta S^{\downarrow,cld} + \Delta F^{\downarrow,cld} - \Delta LE - \Delta H - \Delta N \end{aligned} \tag{5}$$

The overlines denote the average of the two paired experiments. Here, SW and LW radiation are decomposed into clear-sky and cloud (= total-sky – clear-sky) radiative effects. Dividing by $4\sigma\bar{T}^3$ on both sides, the ST change is expressed as the sum of 9 partial-change terms on the right side. It is symbolically written as

$$\Delta T = A + A * SW + SW_{clr} + LW_{clr} + SW_{cld} + LW_{cld} + LH + SH + Q_s \tag{6}$$

The physical meaning of each term is summarized in Table 4. While this diagnosis is made explicitly for the ST change rather than the surface air temperature (SAT) change, it is also helpful to understand the latter, as the two variables are thermally coupled. Indeed, changes in these two variables are nearly identical across all pairs of experiments compared in this study. Nevertheless, care must be exercised in the physical interpretation. For example, upward sensible heat flux cools the surface yet warms the air above. The upward heat flux from the subsurface to the surface represents the warming effect on the surface, which may be transferred to sensible and latent heat fluxes, warming the air above. Therefore, a warming from the subsurface term and a cooling from the evaporation and sensible terms imply atmospheric warming due to the release of heat from the ocean.

Table 4: Physical meaning of individual terms in the analysis of partial surface temperature change

Symbols	The effect of perturbed component at the surface
A	Albedo
$A * SW$	Synergy of albedo and downward SW radiation
SW_{clr}	Clear-sky downward SW radiation
LW_{clr}	Clear-sky downward LW radiation
SW_{cld}	SW cloud radiative effect
LW_{cld}	LW cloud radiative effect
LH	Latent heat due to evaporation
SH	Sensible heat
Q_s	Heat storage in the subsurface (and energy consumed for surface melting)

5 Result

5.1 Impact of cloud parameterization on the preindustrial climate simulation

Figure 2 shows the difference in annual mean SAT between PIvL and PIvS, highlighting the impact of cloud parameterization on preindustrial simulations. The global, annual mean SAT is 13.9°C and 14.6°C in PIvS and PIvL, respectively. Note that comparisons with a global atmospheric reanalysis dataset are presented in Fig. A1. PIvL is generally warmer than PIvS, except in regions around Antarctica, as discussed in Sect. 6. This spatial pattern difference is similar to what was shown in Sherriff-Tadano et al. (2023), in which observed modern vegetation is prescribed. The warmer tropics in PIvL than PIvS are attributable to more solar radiation reaching the surface due to less cloud amount (not shown), which is caused by the higher efficiency of autoconversion rate with the cloud parameter set L (Sect. 2.2). In the Arctic region, defined here as north of 60°N, PIvL is warmer than PIvS by 1.1°C. There is, however, little difference in the simulated vegetation distribution between PIvS and PIvL (Figs. 3a and 3b). We note that the PIvS vegetation is consistent with O'ishi

et al. (2021), which used the identical cloud parameterization but a slightly different value for the ocean's eddy isopycnal thickness diffusivity of the Gent-McWilliams parameterization. Factors contributing to the Arctic SAT difference between the two cloud parameterizations were not investigated in Sherriff-Tadano et al. (2023), which focused on the Southern Ocean. Figure 4 shows the partial contribution of individual components to the total ST difference in the Arctic, as diagnosed by the diagnosis method described in Sect. 4.2. Note that the SAT difference is almost indistinguishable from the ST difference (not shown). The ST difference stands out from October to January, with a peak in November (2.8°C). Conversely, the difference diminishes during the summer. The figure shows a dominant positive contribution from the LW cloud radiative effect, although the SW cloud radiative effect is not negligible in some months.

When focused on the November SAT in the region north of 70°N, covering most of the Arctic Ocean, PIvL (-17.43°C) appears to be a better match to the ECMWF ERA5 reanalysis dataset (-17.62°C for 1980-1999, Hersbach et al., 2020) than PIvS (-19.89°C). However, as Sime et al. (2025) stress, it is important to consider the differences between present-day and preindustrial conditions. The difference between the 1980-1999 average and the 1850-1899 average is 1.05°C in the long-term NOAA 20CRv3 reanalysis dataset (Slivinski et al., 2021). Thus, PIvL and PIvS may contain a similar magnitude of errors of about 1°C with opposite signs. Note that the 1980-1999 average differs by 1.29°C between ERA5 and 20CRv3 reanalyses, which is comparable to, or slightly larger than, the estimated model biases.

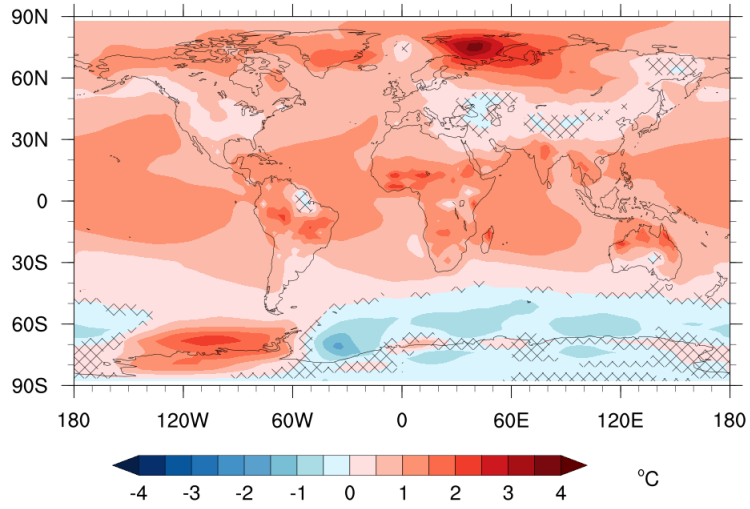

Figure 2: Difference in annual mean SAT between PIvL and PIvS (°C). Grid cells for which the difference is not statistically significant at the 5% level are hatched.

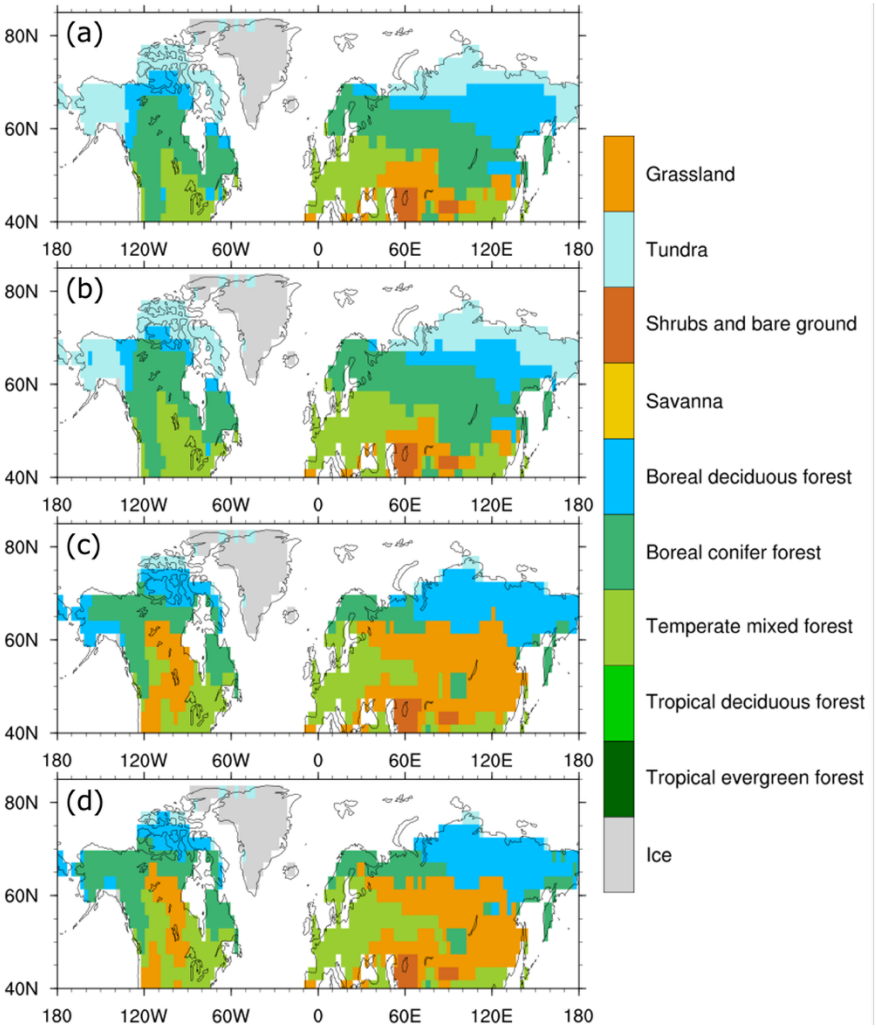

Figure 3: Simulated vegetation distribution: (a) PIvS; (b) PIvL; (c) LIGvS; and (d) LIGvL. These maps show the dominant (most frequent) vegetation type in each grid cell over the last 100 years of the integrations. Note that each grid cell is occupied by a single vegetation type, although this may vary over time.

270

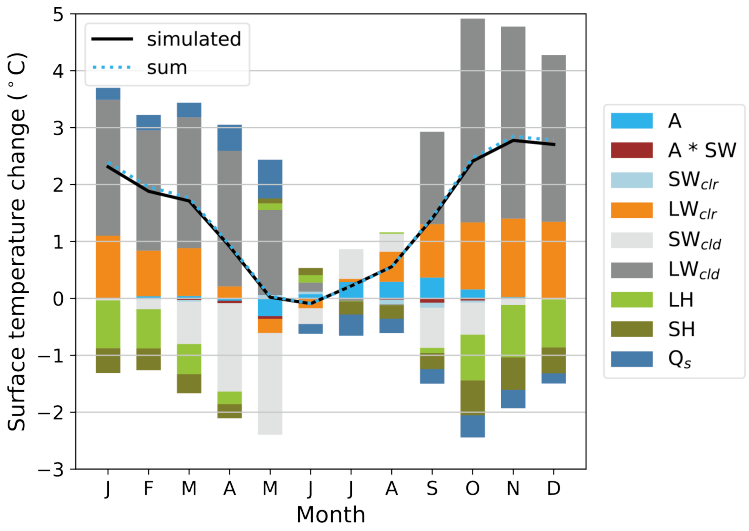

Figure 4: Attribution of Arctic (60-90°N) ST difference to feedback components between PIvL and PIvS (°C). Please refer to Table 4 for a description of each component. In the stacked vertical bars, the positive contributions are shown above the zero horizontal line and the negative ones below. The solid black polygonal line denotes simulation, and the dashed blue line indicates the sum of the diagnosed partial temperature differences, i.e., the cumulative value of the vertical bars.

Figure 5 shows annual mean differences in cloud liquid water path (LWP) and low-level cloud cover for the Arctic between PIvL and PIvS. Except for the northern North Atlantic, larger LWP and low-level cloud cover are simulated in PIvL than PIvS. The larger LWP in PIvL was expected as SLF is parameterized to be larger below 0°C in PIvL compared to PIvS (Sect. 2.2). As the precipitation efficiency is significantly lower for cloud water than for cloud ice in the model (Fig. S1), the average lifetime of cloud water becomes longer. Consequently, the Arctic low-level cloud cover also increases in PIvL compared to PIvS. The final simulated difference, of course, is modified by feedback, such as changes in sea ice cover. The difference in low-level cloud cover is far more pronounced than that of middle and high clouds (not shown). Additionally, the downward LW radiation from low-level clouds is more effective in warming the surface, as the emission temperature at lower altitudes is higher than at higher altitudes. The dominant influence of temperature-cloud phase parameter, rather than other perturbed cloud parameters was verified with additional AGCM experiments and described in Appendix A.

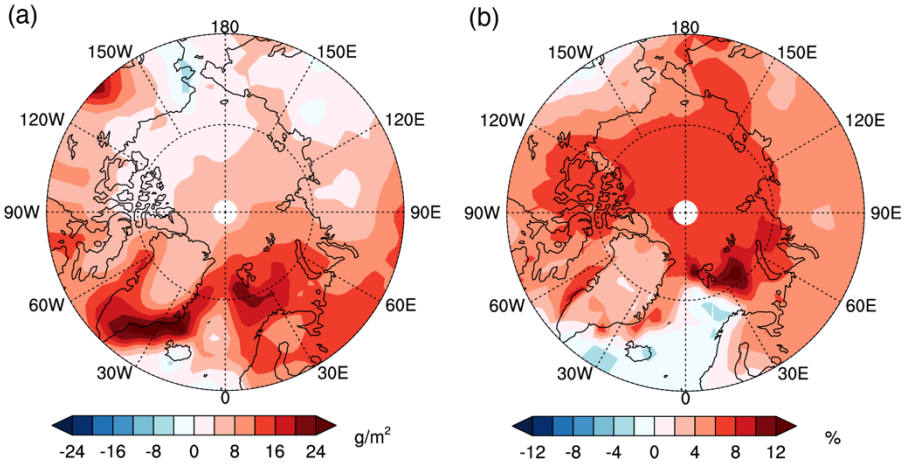

Figure 5: (a) Difference in annual mean liquid water path between PIvL and PIvS (g/m^2); (b) same as in (a) but for low-level cloud cover (%).

290

Figures 6a and 6b show September sea-ice concentrations for PIvS and PIvL, respectively. Note that the minimum in sea ice area occurs in August (ice extent is comparable between August and September) in the PI simulations; September was shown here for the later comparison because it is the month of minimum sea ice area/extent in the LIG simulations. The smaller area of sea ice cover in PIvL than PIvS is consistent with the warmer Arctic in PIvL. Additionally, the sea ice of 295 PIvL is overall thinner than that of PIvS, with a difference of up to 30 cm in the Central Arctic (Figs. 7a and 7b). This difference in sea ice thickness is later shown to be important to understanding the sea ice distribution difference in LIG simulations.

The cold bias and excessive sea ice cover in the Barents and Kara Seas show some improvement in PIvL compared to PIvS, based on sea ice and global atmospheric reanalysis datasets (HadISST2 – Titchner et al., 2014, and ERA5 in Fig. A1, 300 respectively). We note, however, that both versions suffer equally from a significant warm bias over North America (Fig. A1) and a lack of Arctic sea ice along the North American coast, regardless of the applied cloud parameterization.

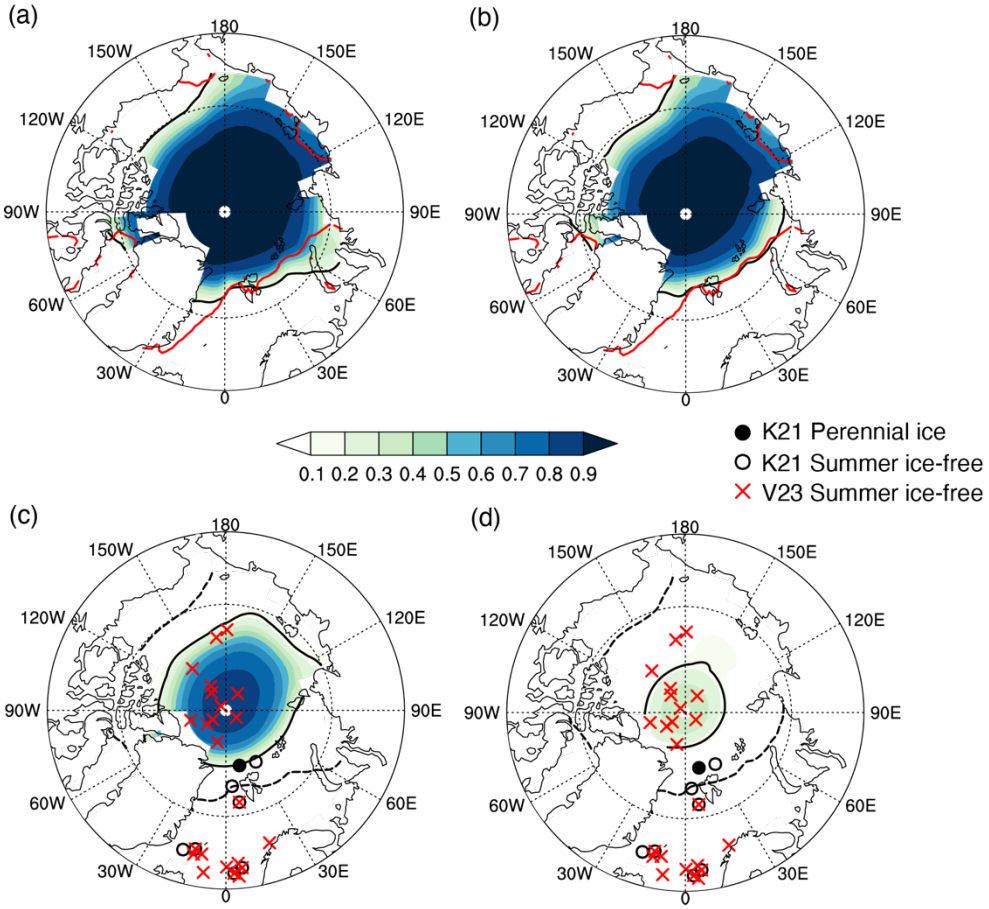

Figure 6: September sea-ice concentration in the Arctic: (a) PIvS; (b) PIvL; (c) LIGvS; and (d) LIGvL. In (a) and (b), black lines denote the simulated boundaries for the ice concentration of 0.15, while red lines denote the observed ones (HadISST2 by Titchner and Rayner, 2014). In (c) and (d), black solid lines denote the simulated boundaries for the ice concentration of 0.15, while black dashed lines denote those in the corresponding preindustrial simulations. The year-round ice cover (solid circles) and summer ice-free conditions (empty circles) suggested by proxy data from Kageyama et al. (2021), and summer ice-free conditions (red cross marks) from Vermassen et al. (2023) are also plotted. Note that only proxies claimed as good chronological control are shown for Kageyama et al. (2021), and whether the data from Vermassen et al. (2023) actually represent LIG has been questioned, as stated in the Introduction.

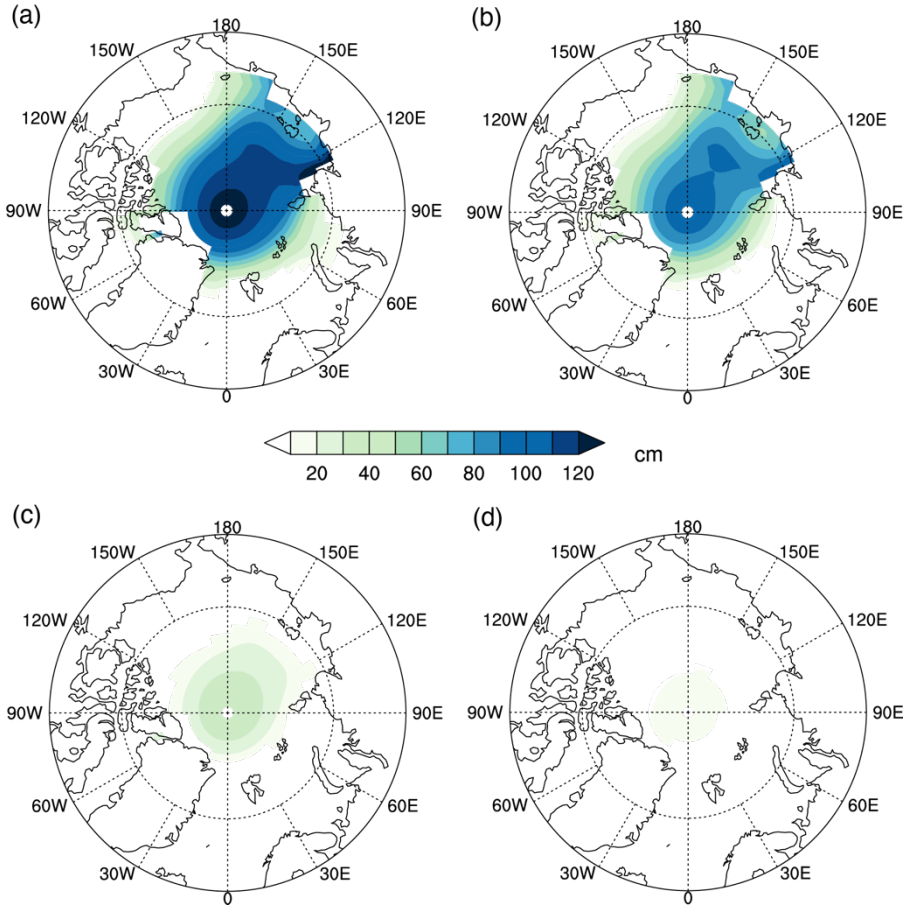

Figure 7: September sea-ice thickness (cm) in the Arctic: (a) PIvS; (b) PIvL; (c) LIGvS; and (d) LIGvL.

315

5.2 Comparison of LIG simulations with proxies

Figures 8a and 8b show the difference in summer SAT between the LIG and PI simulations. The estimate from proxy records (Guarino and Sime, 2022) is also presented. Note that this family of proxy datasets has been used previously and updated for the model-data comparison (CAPE, 2006; Guarino et al., 2020; Sime et al., 2023). Both ΔLIGvS and ΔLIGvL
320 generally capture the strong summer warming at LIG, with some overestimation over Alaska and underestimation over Greenland. The root mean squared error is 1.8 °C for ΔLIGvS and 1.9 °C for ΔLIGvL, and they are comparable. It is difficult to draw a definitive conclusion about the superiority, given the uncertainty in proxy reconstructions and the limited number of sample locations.

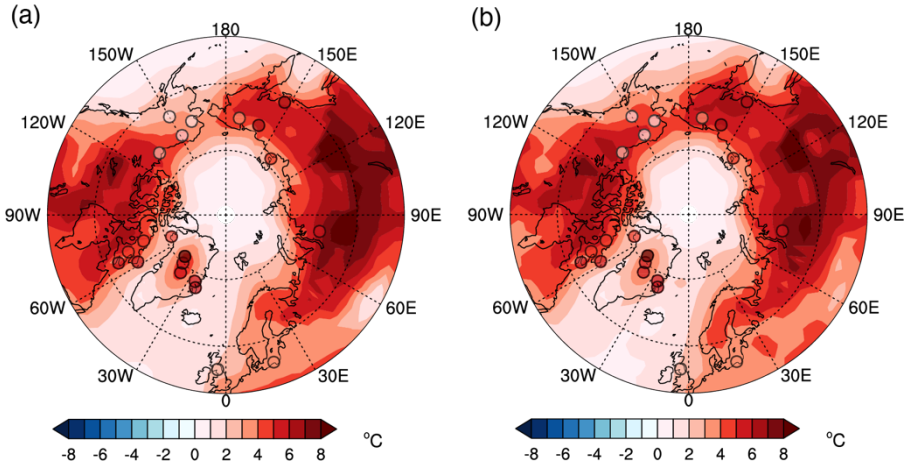

Figure 8: Comparison of simulations with proxies for the ΔLIG (LIG – PI) summer SAT difference (June-July-August): (a) ΔLIGvS; and (b) ΔLIGvL. The circles represent proxy data from Guarino and Sime (2022).

The annual mean SAT at LIG is warmer than PI in the Arctic (to the north of 60°N) by 2.7°C for ΔLIGvS and by 3.1°C for ΔLIGvL, slightly larger with the cloud parameter set L. It is also compared with the proxy-based estimate (Turney and Jones, 2010; Capron et al., 2017) in Fig. S7. It is important to note that the dataset of Turney and Jones (2010) was compiled from the locally warmest timing within a wide period spanning approximately 13,000 years, from 129 to 116 kaBP. The assumption that peak warmth at LIG was simultaneous has been challenged, and the validity of comparison with 127 kaBP simulations for the model assessment has been questioned (Capron et al., 2014, 2017). Nevertheless, the comparison is referenced here because the impact of cloud phase representation on SAT is more critical in winter, rather than summer, and it is important to point out that the discrepancy of simulation with this dataset, shown by O'ishi et al. (2021), remains substantial even with the alternative cloud phase representation. We must wait for a well-dated dataset for a more quantitatively solid comparison.

Figures 6c and 6d show September sea-ice concentration for LIG simulations, LIGvS and LIGvL, respectively. The area of sea ice cover decreases compared to the corresponding PI simulations. The reduction of sea ice cover in LIGvL is, however, much more drastic than that in LIGvS. Figures 6c and 6d compare two different sea ice cover reconstruction datasets with these LIG simulations: Kageyama et al. (2021) and Vermassen et al. (2023). At one location (PS92/039-2: 81.92°N, 13.83°E) identified as ice-covered in summer by the Kageyama et al. (2021) compilation, sea ice is present in LIGvS but absent in LIGvL simulations. On the contrary, overall simulated sea ice cover in LIGvL is much closer to the Vermassen et al. (2023) compilation and a nearly ice-free summer Arctic suggested by Malmierca-Vallet et al. (2018) and Sime et al. (2023) than LIGvS. Notice that the difference in ice thickness in the Central Arctic between LIGvS and LIGvL is as much as 27 cm (Figs. 7c and 7d), which is close to the difference between PIvS and PIvL (Figs. 7a and 7b). This implies that whether sea ice remains in summer at LIG in these simulations is sensitive to the simulated sea ice thickness under

modern conditions. In addition, the annual mean Arctic warming for ΔLIGvL is larger than that for ΔLIGvS, which may further help to simulate a smaller summer sea ice cover in LIGvL.

5.3 Causes of the Arctic warming at LIG

As discussed in Sect. 5.2, there is a discernible annual mean SAT difference between ΔLIGvL and ΔLIGvS. Nevertheless, the simulated vegetation distributions for LIGvS and LIGvL are similar, in which the area covered by tundra at NH high latitudes in PI simulations is replaced by boreal deciduous forest in LIG simulations (Figs. 3c and 3d). Similarly, the area covered by boreal conifer forest at NH mid-latitudes in PI simulations is replaced by grassland in LIG simulations. The former change is particularly effective at altering surface albedo and the consequent warming, as discussed by O'ishi et al. (2021).

Figure 9a shows the partial contribution of individual components to the total ST difference over the Arctic Ocean for ΔLIGvS according to the diagnosis method described in Sect. 4.2. LIGvS is warmer than PIvS in the Arctic from April to December, with a peak warming in October. From May to August, the dominant warming factors are changes in downward clear-sky SW and LW radiation and in surface albedo. The increase in clear-sky SW radiation is expected and reflects differences in summer insolation at the top of the atmosphere (TOA) driven by variations in astronomical parameters. The increase in clear-sky LW radiation is caused by increased air temperature and/or water vapor. The net decrease in subsurface heat uptake (positive Q_s term) and the net increase in upward surface latent and sensible heat fluxes (negative LH and SH terms), which are respectively tagged with surface warming and cooling from October to December, imply atmospheric warming via heat transfer from the ocean to the atmosphere. The mechanism of warming involving these processes is consistent with many previous studies: stronger insolation at LIG reduces sea ice cover, and the ocean mixed layer absorbs more heat in summer and releases it to the atmosphere in autumn-winter (e.g., O'ishi et al., 2021; Sicard et al., 2022; Hirose et al., 2025). It is important to note that the LW cloud radiative effect contribution to surface warming is not negligible from September to November, consistent with the increase in low-level cloud cover in autumn (Fig. 10a).

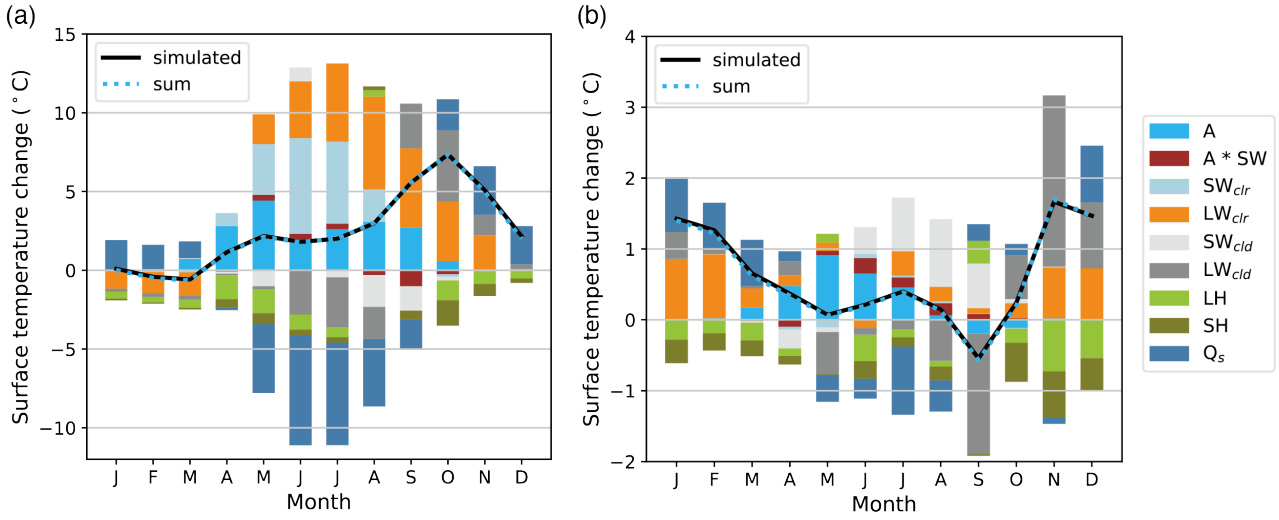

Figure 9: Attribution of Arctic Ocean (60-90°N) ST difference to feedback components (°C): (a) ΔLIGvS (LIGvS – PIvS); and (b) ΔLIGvL – ΔLIGvS. Please see Table 4 for the description of each component. In the stacked vertical bars, the positive contributions are shown above the zero horizontal line and the negative ones below. The solid black polygonal line denotes simulation, and the dashed blue line indicates the sum of the diagnosed partial temperature differences, i.e., the cumulative value of the vertical bars.

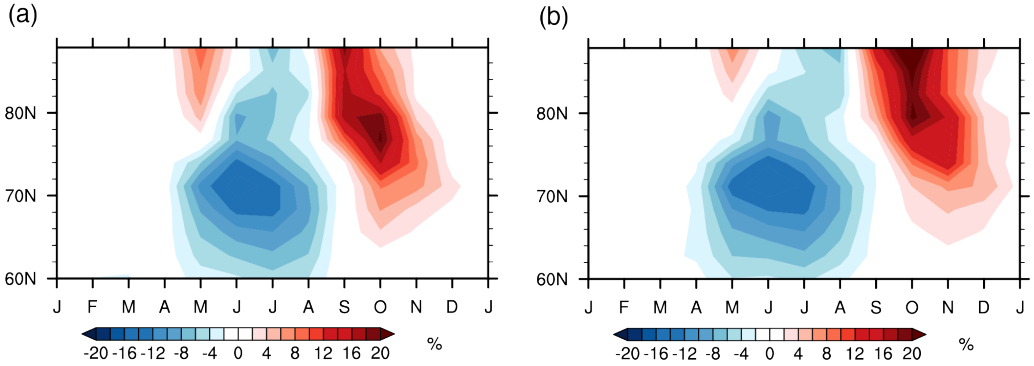

Figure 10: Difference in zonal and monthly mean low-level cloud cover between LIG and PI (%): (a) ΔLIGvS; and (b) ΔLIGvL.

Figure 11 shows the changes in sea ice concentration in August and September and low-level cloud cover in September and October for ΔLIGvS (north of 60°N). It appears that regions of sea ice retreat in August and September loosely coincide with the areas of cloud increase in September and October, respectively. The match is firmer in the zonally elongated region to the north of Spitsbergen and the region from the Laptev Sea to the Canadian Archipelago in Figs. 11b and 11d. While we do not fully understand the reason for this one-month delay in response, the previous study by Abe et al. (2016) reported a similar relationship between shrinking sea ice and increasing cloud cover in a 1976-2005 simulation using a different version of the MIROC model. In their study, a decrease in September sea-ice cover leads to increased upward heat and moisture

fluxes through the open-water surface. As the air-sea temperature difference rises in October, these fluxes further intensify, resulting in an apparent one-month lag between the decrease in sea ice and the increase in cloud cover. Although radiative forcing and climate conditions differ from ours, Fig. 11 is qualitatively consistent with their argument.

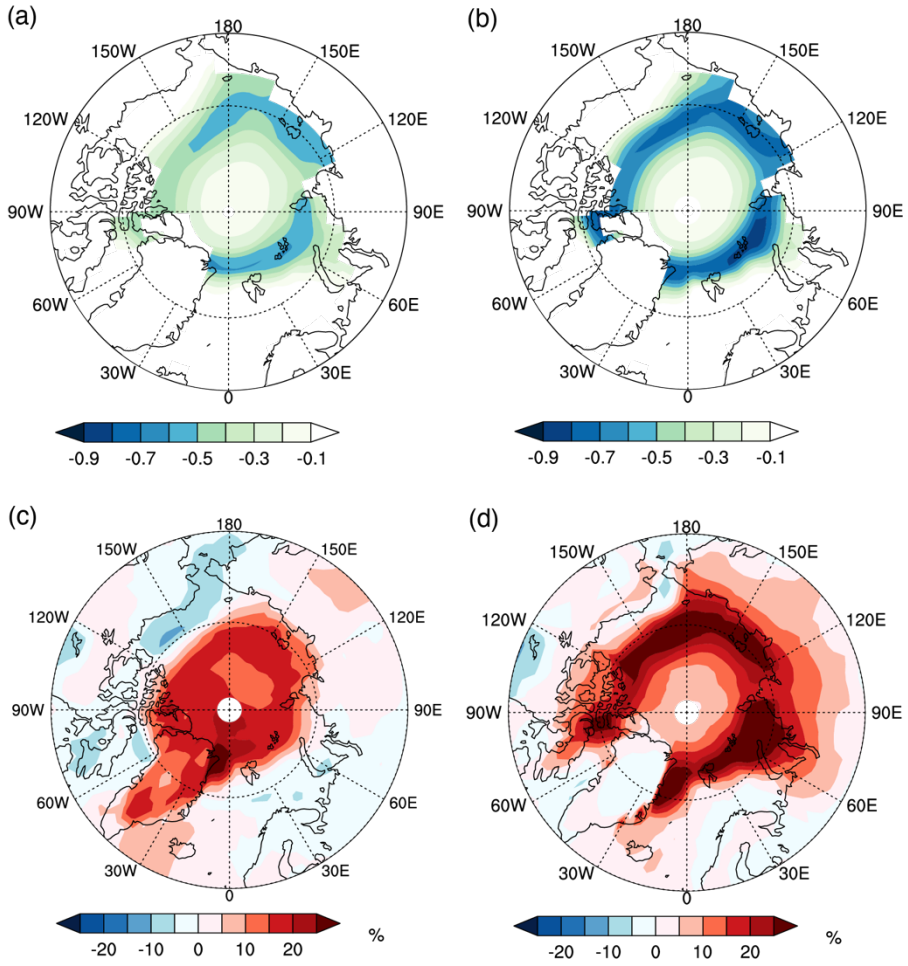

Figure 11: Changes in sea ice concentration and low-level cloud cover for ΔLIGvS: (a) August ice concentration; (b) September ice concentration; (c) September cloud cover (%); and (d) October cloud cover (%).

The description above is consistent with the seasonal evolution of atmospheric and upper-ocean temperature anomalies shown in Fig. 12a, where anomalous ocean heat content increases in summer and decreases in autumn. It is worth noting that summer warming extends to the upper troposphere, whereas autumnal warming is confined to the near-surface layers, qualitatively consistent with Sicard et al. (2022, Fig. 8). In winter, warming is slight in the ocean, and cooling occurs in the atmosphere.

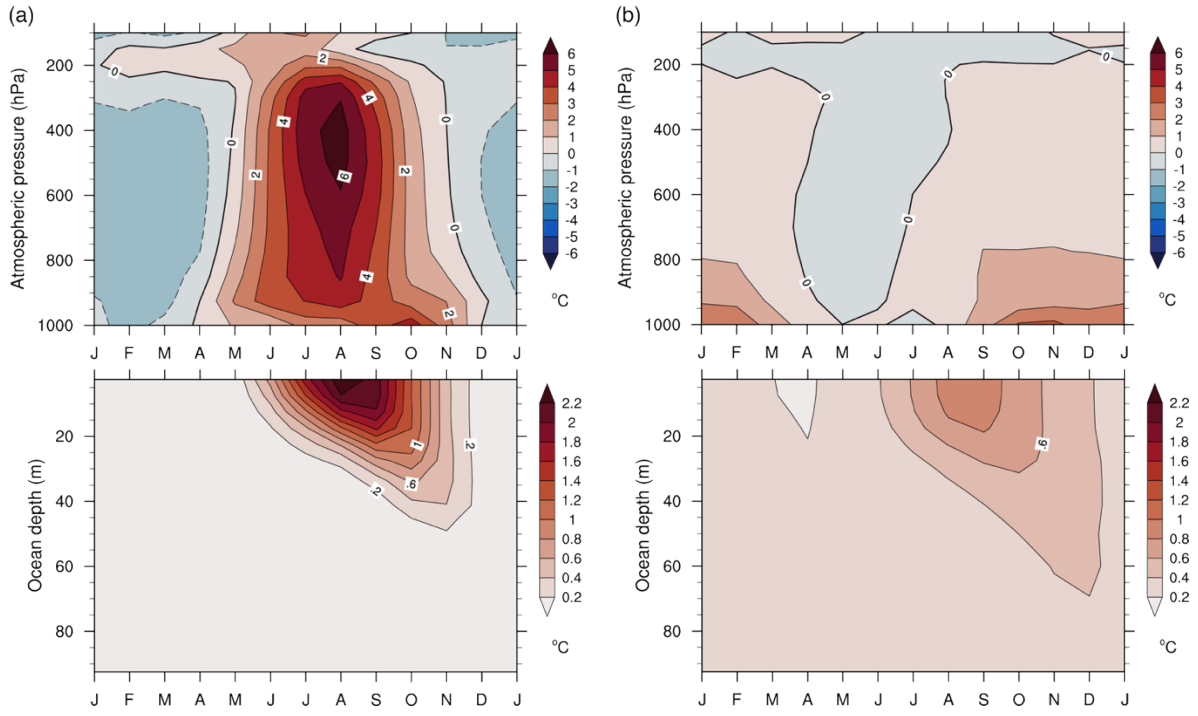

Figure 12: Temperature anomalies in the atmosphere and the upper ocean (°C): (a) ΔLIGvS; and (b) ΔLIGvL – ΔLIGvS. The regional average is taken for the Arctic Ocean (60-90°N).

5.4 Impact of cloud parameterization on LIG climate simulations

Figure 9b shows the partial contribution of individual components to the total ST difference in the Arctic for the difference between ΔLIGvL and ΔLIGvS. The net increase in subsurface ocean heat content in summer (negative Q_s term), along with the albedo feedback (positive A term), and the net decrease in subsurface ocean heat content in winter (positive Q_s term), indicate enhanced heat exchange between the ocean and the atmosphere with reduced sea ice cover. From October to December, the difference between ΔLIGvL and ΔLIGvS is caused primarily via downward LW cloud radiative effect, consistent with a marked difference in low-level cloud cover increase in ΔLIGvL (Fig. 10b) than ΔLIGvS (Fig. 10a). Figures 13a and 13b show difference of the difference, i.e., ΔLIGvL – ΔLIGvS, in LWP and low-level cloud cover, respectively, for the average from October to December. The overall positive anomalies are observed. As discussed above, the increases in LWP and low-level cloud cover in LIG simulations are likely associated with decreased sea ice cover relative to PI simulations. As the reduction in sea ice cover is much larger in ΔLIGvL than in ΔLIGvS, a larger cloud response occurs in ΔLIGvL than in ΔLIGvS. In addition, air temperatures drop below -15°C in November and December across large areas of the Arctic, even near the surface at LIG. As the cloud parameterization allows SLF to have non-zero values below -15°C only in the cloud parameter set L, the distinct increase in LWP in the LIG simulation compared to the PI simulation is

observed for ΔLIGvL in November and December. Therefore, the positive anomalies in Figs. 13a and 13b are simulated due to a larger decrease in sea ice cover (Fig. 13c) and the allowance of mixed-phase clouds at lower temperatures by the cloud parameter set L. The dominant influence of the temperature-cloud phase parameter, rather than other perturbed cloud parameters, was verified through additional AGCM experiments and is described in Appendix A.

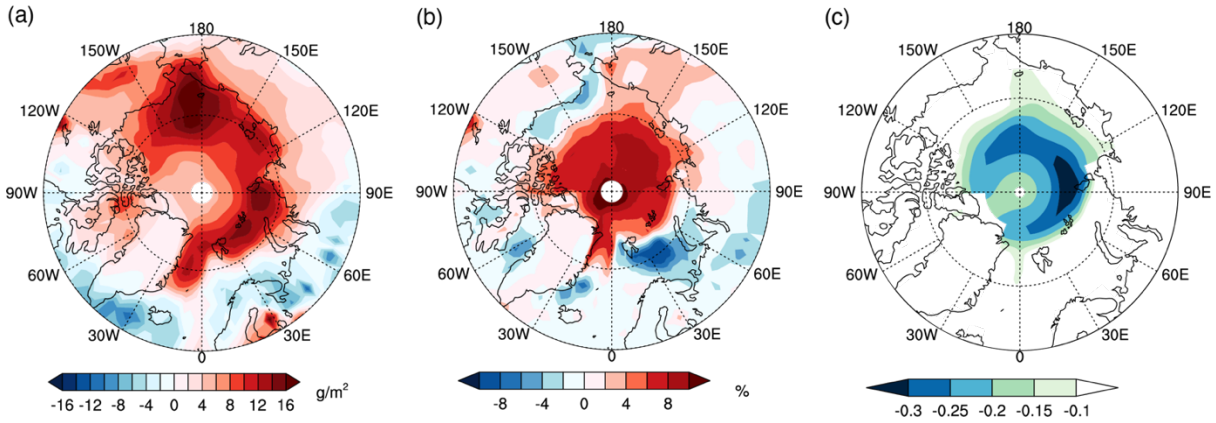

Figure 13: Difference between ΔLIGvL and ΔLIGvS: (a) liquid water path (from October to December); (b) low-level cloud cover (from October to December); and (c) sea ice concentration (from September to November).

The description above is consistent with the seasonal evolution of atmospheric and upper-ocean temperature anomalies shown in Fig. 12b, where anomalous ocean heat content increases in summer and decreases in autumn. The contrasting weaker summer and stronger winter signals in the ocean temperature in Fig. 12b, relative to Fig. 12a, are striking. The warming signal is also evident in the winter atmosphere in Fig. 12b. These signatures may be related to the cloud-phase feedback, which helps sustain the positive ocean temperature anomaly through winter and thereby potentially impacts sea ice growth. Both a larger reduction in sea ice cover and stronger cloud feedback in the model with cloud parameter set L functionally contribute to warmer conditions relative to the model with cloud parameter set S. However, given the limitations in disentangling both effects in coupled atmosphere-ocean model simulations, each effect, particularly on sea ice growth and loss, is not quantified separately in the current study. The model capable of ice mass tendency diagnostics, as suggested by Keen et al. (2021) and Sime et al. (2025), would help explore this aspect.

6 Discussions

Is the representation of cloud phase also crucial for the model without dynamic vegetation feedback? Many CMIP6-PMIP4 climate models do not account for geographical changes in vegetation types. Here, we examine whether the temperature dependence of cloud phase has a similar impact in these models to that observed above. We have confirmed that the MIROC4m model with the cloud parameter set L shows a warmer Arctic than the model with the parameter set S for the

PI simulations (PIfL and PIfS, respectively), and thinner sea ice thickness in September by as much as 27 cm in the Central Arctic (Fig. S5), slightly less than the difference between PIvL and PIvS. Regarding the changes from PI to LIG (ΔLIG), the annual mean SAT increase was suppressed to 1.7°C for ΔLIGfS and 1.8°C for ΔLIGfL, due to the lack of vegetation feedback. Nevertheless, it is common for the winter warming over the Arctic Ocean to be larger in ΔLIGfL due to the increase in low-level cloud cover, and for the sea ice area to decrease significantly in summer at LIG with the cloud parameter set L (Fig. S8). Therefore, even if many models do not incorporate a dynamic-vegetation component, the temperature dependence of cloud phase can be an essential source of uncertainty for LIG simulations.

What is the relative importance of cloud phase representation and dynamic vegetation feedback, and how do they potentially affect the model spread at LIG? We added four values of summer (August-September) sea ice area (LIGvS, LIGvL, LIGfS, and LIGfL) to the multi-model data (Kageyama et al., 2021) shown in Fig. 14. The summer Arctic sea-ice area in LIGvL is the second smallest, after that of HadGEM3-GC31-LL, the only model that reproduces a climatologically and practically ice-free summer Arctic with explicit melt-pond representation. Sea ice areas in LIGvS and LIGfL are relatively close to the LIG sea ice values in CESM2 and NESM3. These results suggest that the temperature dependency of cloud phase may contribute to part of the model spread for LIG simulations. Additionally, the magnitude of the cloud-phase effect is comparable to, or even exceeds, that of dynamic vegetation feedback. The current study thus suggests that cloud-phase and vegetation feedback are essential components to investigate, alongside the role of melt ponds. The melt-pond feedback accelerates summer ice melt through the albedo effect. Excessive heat is stored in the ocean mixed layer, amplifying the autumn-winter warming through its release (Diamond et al., 2021, 2024; Guarino et al., 2020; Kageyama et al., 2021; Sime et al., 2025). As cloud-phase feedback is enhanced by reduced sea ice cover and amplifies surface warming via the greenhouse effect during a relatively cold season, both feedbacks may act constructively to amplify Arctic warming at LIG.

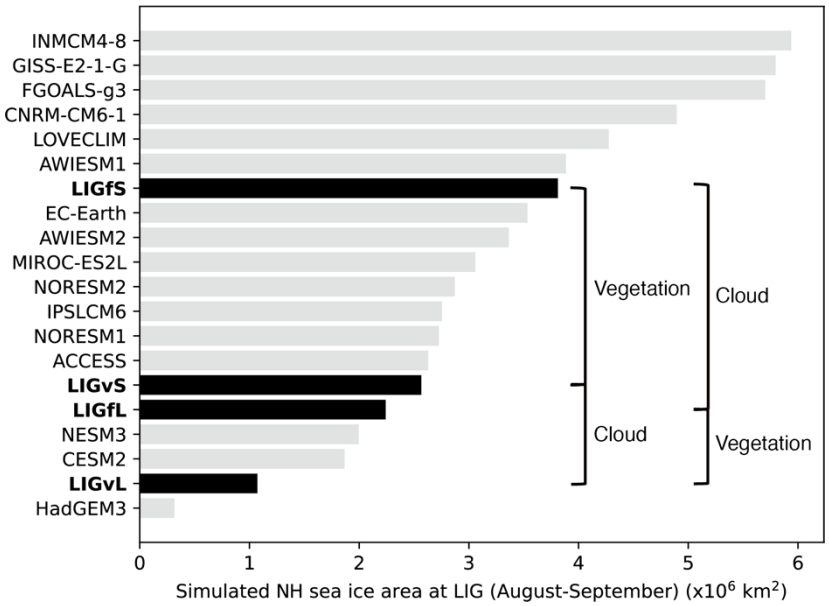

Figure 14: Simulated NH sea ice area at LIG (August-September). The values of other models (gray bars) are taken from the Supplementary data of Kageyama et al. (2021). "Vegetation" and "Cloud" denote the effects of dynamic-vegetation feedback and cloud parameterization, respectively, as examined in the present study.

The significant warm bias over North America and insufficient sea ice along the North American coast are concerns in attributing the simulated results. It is admittedly tricky to disentangle the effects of model bias in modern climate and cloud feedback induced by LIG forcing because they are interconnected. Therefore, care must be exercised when interpreting and drawing implications from our results. Here, we review the models' performance and clarify our intent and message. Sea ice concentration in September, when sea ice is at its minimum in LIG simulations, improves in PIvL relative to PIvS, notably in the Barents and Kara Seas. The most significant difference in SAT between PIvL and PIvS occurs in November, and the magnitude of the biases over the Arctic is comparable, with opposite signs. The difference in low-level cloud cover between PIvL and PIvS is generally smaller than their model biases, indicating room for improvement in cloud variables. While the cloud distribution was examined in Sherriff-Tadano et al. (2023), the absence of a COSP simulator (Bodas-Salcedo et al. 2011) in this model version prevents a rigorous comparison of cloud phases with satellite observations. The summer SAT anomaly of LIG simulations relative to PI simulations in both models exhibits almost the same root mean squared errors when compared with the limited available proxy reconstructions. The annual mean SAT anomaly in LIG simulations relative to PI simulations indicates improved performance for cloud parameter set L. However, the assumption made about the proxy compilation precludes a confident judgment of superiority. Nevertheless, it remains a valid concern that both models may substantially underestimate the annual mean response to LIG forcing.

We point out that simulated modern sea ice thickness has not yet received sufficient attention in interpreting paleoclimate simulations, perhaps due to the lack of a long-term observational dataset of sea ice thickness. Our models generally fail to

reproduce observed thicker Arctic ice near the Canadian Archipelago and Greenland because of the zonal distribution induced by polar Fourier filtering. The reduction in sea ice cover increases the moisture supply to the atmosphere, thereby increasing low-level cloud cover and the LW cloud radiative effect. The thinner baseline sea ice at PI may lead to greater sea ice melt and consequently to enhanced LW cloud feedback at LIG. On the other hand, already insufficient sea ice along the North American coast at the PI baseline may have only a minor local impact on subsequent changes in sea ice cover and LW cloud feedback at LIG. Because the melting temperature of ice is virtually constant, we cannot rule out that model biases partly promote the simulated ice-free Arctic summer. The relationship among sea ice extent, sea ice thickness, and cloud feedback warrants further investigation and is likely to be valuable with newer versions of the model that do not require polar filtering, as well as in a multi-model context.

Given model biases, our intention is not to declare that either of our simulations is successful, but rather to present cases in which the representation of the temperature dependency of cloud phase substantially affects the LIG Arctic simulations and can also be a contributing factor, or at least a factor to be concerned about, to the existing and unexplained large model spread. This underscores the need for multi-model analysis of cloud-phase feedback. There are a couple of other reasons why we did not claim which model version is more correct: 1) While the temperature dependency of cloud phase in the parameter set L is designed to be closer to modern satellite observations in the previous study (Sherriff-Tadano et al., 2023), there is no guarantee that the same relation holds at the LIG environment, when the aerosol distribution is likely different from that of the present-day. Thus, we intended to emphasize that the aim of the study has a nature of sensitivity experiments; 2) the agreement of annual mean SAT difference of LIG and PI between the model and proxies is still insufficient or the disagreement cannot be rejected, as commonly seen in other models; and 3) while progress has been made, summer sea ice cover at LIG still has uncertainty due to the limited number of well-dated reliable Arctic sea-ice records.

The cloud parameter sets S and L determine the cloud phase for a particular temperature range. Therefore, their impacts on PI simulations are different between the Southern Ocean and the Arctic. Although the Southern Ocean is clearly not the focus of this study, we briefly discuss this asymmetric response between the hemispheres. When the cloud parameter set is changed from S to L, the annual mean SAT over the Arctic increases. At the same time, it decreases in many parts of the Antarctic region, except for the 60°W-150°W longitude range (Fig. 2). The cause of the difference is the cloud parameters, but it is essential to recognize that the equilibrium climate state is determined as a result of feedback through changes in atmospheric circulation, moisture transport, and other factors. Their details are, however, beyond the scope of this paper. The feedback analysis described in Sect. 4.2 is also applied to the Antarctic region (60°S-90°S, excluding longitudes 60°W-150°W). It is found that the difference in downward SW cloud radiative effect from December to February, the summer season in Antarctica, is a dominant contributing factor for the decrease in ST (not shown). In the summer (June to August), Arctic air temperature in most regions with low clouds (below 680 hPa) exceeds 0°C in the two PI experiments. Thus, the difference in temperature dependency of cloud phase between PIvS and PIvL has little effect. On the contrary, in the Antarctic summer (December to February), the air temperature in most regions with low clouds is below 0°C, and hence the difference in temperature dependence of the cloud phase has a profound impact on SLF and cloud cover. SLF is larger over

this temperature range for PIvL, leading to more low-level clouds that reflect strong summer sunshine at high latitudes in the Southern Hemisphere. In short, the asymmetric polar response to the temperature dependence of the cloud phase originates from the different climatological temperatures between the two polar regions.

7 Summary and Conclusions

For the first time, we investigated the influence of cloud-phase representation in LIG simulations by comparing two temperature-dependent relations for SLF. In the cloud parameter set S, the liquid phase cloud can exist only above -15°C, while it can exist as low as -28°C in the cloud parameter set L. Consequently, the SLF is always larger between -28°C and 0°C, and the cloud phase change occurs with a slight temperature perturbation even below -15°C, with the parameter set L.

The AOGCM with a dynamic vegetation component, MIROC4mV, exhibits a warmer Arctic climate for parameter set L than for S, primarily because larger LWP and low-level cloud cover lead to a stronger cloud-induced greenhouse effect in winter. This mechanism is unique to the polar regions, where mixed-phase clouds prevail during the cold seasons, when sunlight is limited. While there is a relatively small difference in sea ice concentration between the two model versions, a notable difference in sea ice thickness of up to 30 cm exists.

LIG simulations with MIROC4mV show slightly larger annual mean warming with parameter set L than with parameter set S, compared to the respective PI simulations. The larger warming is attributed to larger LWP and low-level cloud cover due to the cloud-phase feedback from October to December. The positive cloud-phase feedback is larger with the parameter set L because the reduction in sea ice is greater, and the phase change occurs below -15°C only for this set. With the thinner sea ice at the PI simulation and larger warming at LIG from the PI simulation for the parameter set L, sea ice cover at LIG in September is much smaller with the parameter set L. The parameter set L shows much better agreement with recent studies suggesting an ice-free Arctic in summer, while noting that the model bias exists in both versions. It is somewhat surprising that the difference between the two cloud parameter sets induces greater winter warming in both the near-surface atmosphere and the ocean mixed layer than does LIG radiative forcing.

Since many CMIP6-PMIP4 climate models do not incorporate dynamic vegetation feedback, we also examined the impact of cloud-phase representation using the AOGCM MIROC4m, which lacks the dynamic vegetation component. Although the levels of annual mean warming and reduction of sea ice extent are much more moderate in MIROC4m compared to MIROC4mV, a similar impact of cloud-phase representation is observed, suggesting that the cloud phase representation might be one of the factors that generate differences in multi-model LIG simulations.

Previous studies have highlighted the importance of representing vegetation change in simulating significant annual-mean Arctic warming (O'ishi et al., 2021) and melt ponds on sea ice in simulating ice-free summer Arctic at LIG (Guarino et al., 2020; Diamond et al., 2021). This study adds another source of uncertainty that may help alleviate the underestimation of Arctic warming by current climate models. As the temperature dependency of the cloud phase is controlled by the availability of ice-nucleating particles (and cloud condensation nuclei) in the real world, no universal cloud-phase function

of temperature is expected to exist. The relation is likely to vary with climate state and regions. We argue that refining cloud-phase formulations and improving the reproducibility of present-day sea ice thickness in climate models are essential to improve Arctic simulation at LIG and are likely to be crucial for simulations of future climate.

Code availability

The codes for MIROC4mV and MIROC4m are not publicly archived due to the MIROC community's copyright policy. Readers are requested to contact the corresponding author if they wish to validate the MIROC model configurations and conduct replication experiments.

Data availability

HadISST.2.2.0.0 sea ice data used in Figs. 6 and S8 were downloaded from https://www.metoffice.gov.uk/hadobs/hadisst2/index.html. The summer SAT reconstruction (Guarino and Sime, 2022) used for Figs. 8 and S6 was taken from https://doi.org/10.5285/9AB58D27-596A-472C-A13E-2DCD68612082. The annual mean SAT reconstruction used for Fig. S7 was obtained from the Supporting Information of Turney and Jones (2010) and the Supplementary Data of Capron et al. (2017). The sea ice reconstruction used for Figs. 6 and S8 was obtained from Table 1 of Kageyama et al. (2021) and the Extended Data Table 1 of Vermassen et al. (2023). The ERA5 data used for Fig. A1 were downloaded from the Copernicus Climate Change Service (C3S) Climate Data Store. Neither the European Commission nor ECMWF is responsible for any use that may be made of the Copernicus information or data it contains. The 20CRv3 data were downloaded from https://psl.noaa.gov/data/gridded/data.20thC_ReanV3.html. CALIPSO-GOCCP cloud data used for Figs. A3 and A4 were downloaded from https://climserv.ipsl.polytechnique.fr/cfmip-obs/. We will make our own data publicly available upon acceptance for reproducing the figures.

Author contribution

NA and MY prepared the manuscript and contributed equally to this work, with contributions from all co-authors. MY designed the study, and both NA and MY carried out the experiments and analyses. The part of this paper is based on NA's master's thesis, which MY supervised.

Competing interests

The authors declare that they have no conflict of interest.

Acknowledgments

We thank Louise C. Sime and three anonymous reviewers for their many valuable comments, which substantially improved the manuscript. All computations were performed on the JAMSTEC Earth Simulator 4 supercomputer. We also thank the MIROC model development team for making the model available, and Drs. Takashi Obase and Fuyuki Saito for their technical assistance in deploying the model at the Earth Simulator 4. Figures were created using the NCAR Command Language version 6.6.2 (https://www.ncl.ucar.edu/) and Python3 matplotlib. The AI tool Grammarly was used to help fix grammatical errors in English.

Financial support

This work was supported by the Arctic Challenge for Sustainability Programs, ArCSII (Grant No. JPMXD1420318865) and ArCSIII (Grant No. JPMXD1720251001), and a Grant-in-Aid from JSPS KAKENHI (Grant No. JP19H05595, JP24H00256, and JP24H02346). TO was supported by MEXT program for the advanced studies of climate change projection (SENTAN) Grant Number JPMXD0722680395.

Appendix A: Model bias

Simulated SAT, sea ice concentration, and low-level cloud cover, which are of primary interest in the current study, are compared with the observational datasets. These comparisons are not rigorous because the observations pertain to the present-day state, which differs from the preindustrial state; however, we examined the potential impact of this difference using the available simulation data. Historical simulations are available only for one model version with 3 ensemble members (Yoshimori et al., 2018), namely the model with cloud parameter set S and without the dynamic vegetation component. Note that our vegetation-coupled climate model has not been used to investigate short-term transient climate response. In MIROC4mV, the dynamic vegetation component was incorporated into the atmosphere-ocean model MIROC4m, enabling it to simulate vegetation response to the mean climate (as it responds to the last 20-year average climatology during the integration), but its response to climate trends has not been thoroughly examined.

The comparison of the SAT is presented in Fig. A1. A significant warm bias is seen in North America, the northern coast of Alaska, and Greenland. Therefore, care must be exercised when investigating climatic responses in these regions. The error in the Central Arctic is comparatively small, and PIvL generally performs better there and at high latitudes of Eurasia (Figs. A1a and A1b). The distinction between present-day and preindustrial conditions does not significantly affect these interpretations (Fig. A1c). The comparison of the sea ice concentration is presented in Figs. 6a and 6b, and is described in the main text. Thus, only the difference between the present-day and preindustrial conditions is presented in Fig. A2. The difference in the Barents Sea is not negligible. Still, it is difficult to relate the distinction between present-day and preindustrial conditions to PIvS (or PIvL) because ice cover there is already small in models with dynamic vegetation.

The comparison of low-level cloud cover is shown in Fig. A3. While some large-scale spatial patterns are reasonably captured, both PIvS and PIvL generally underestimate cloud cover relative to satellite observations. While the cloud distribution was examined in Sherriff-Tadano et al. (2023), the absence of a COSP simulator (Bodas-Salcedo et al. 2011) in this model version prevents a rigorous comparison with satellite observations. Fig. A4 shows the seasonal variations of low-level cloud cover, where both PIvS and PIvL miss the secondary peak in autumn. Although missing observational data in the Central Arctic render the evaluation inconclusive, the alternative cloud parameterization examined in the current study does not resolve many of the biases in cloud distribution. Reproducing cloud variables more accurately remains a significant challenge in model development, as in other models.

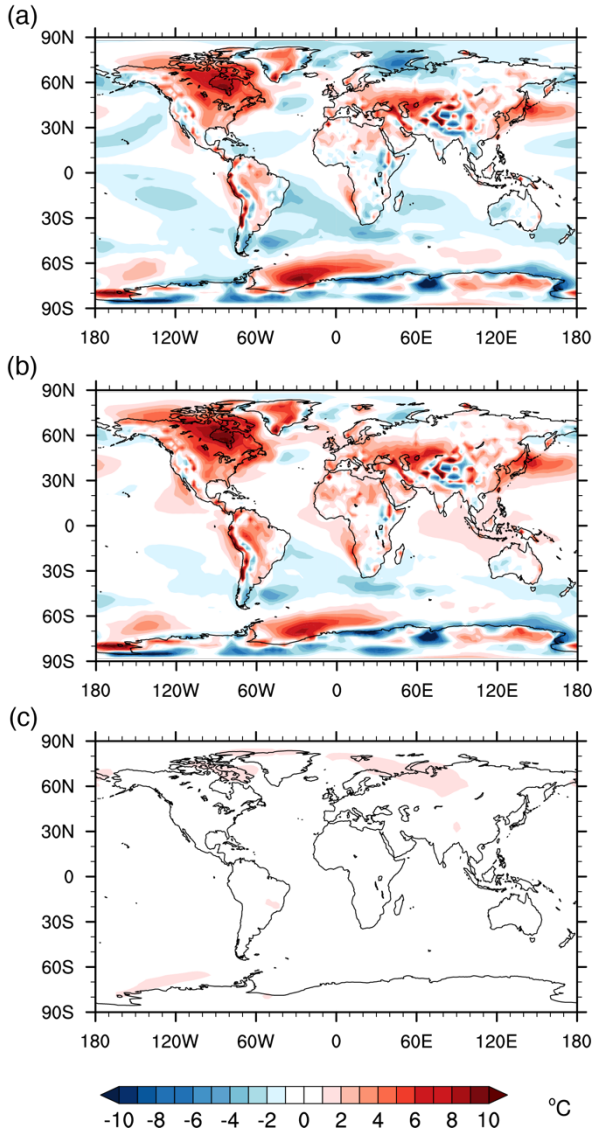

Figure A1: Difference in annual mean SAT: (a) PIvS and the global reanalysis dataset ERA5 (Hersbach et al., 2020); (b) as in (a) but for PIvL; and (c) 1980-1999 in the historical and preindustrial simulations of Yoshimori et al. (2018) (°C). ERA5 data represent the average of 20 years (1980-1999).

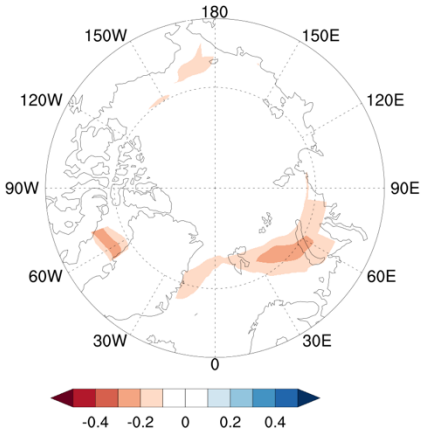

Figure A2: Difference in September sea ice concentration between 1980-1999 in the historical and preindustrial simulations of Yoshimori et al. (2018).

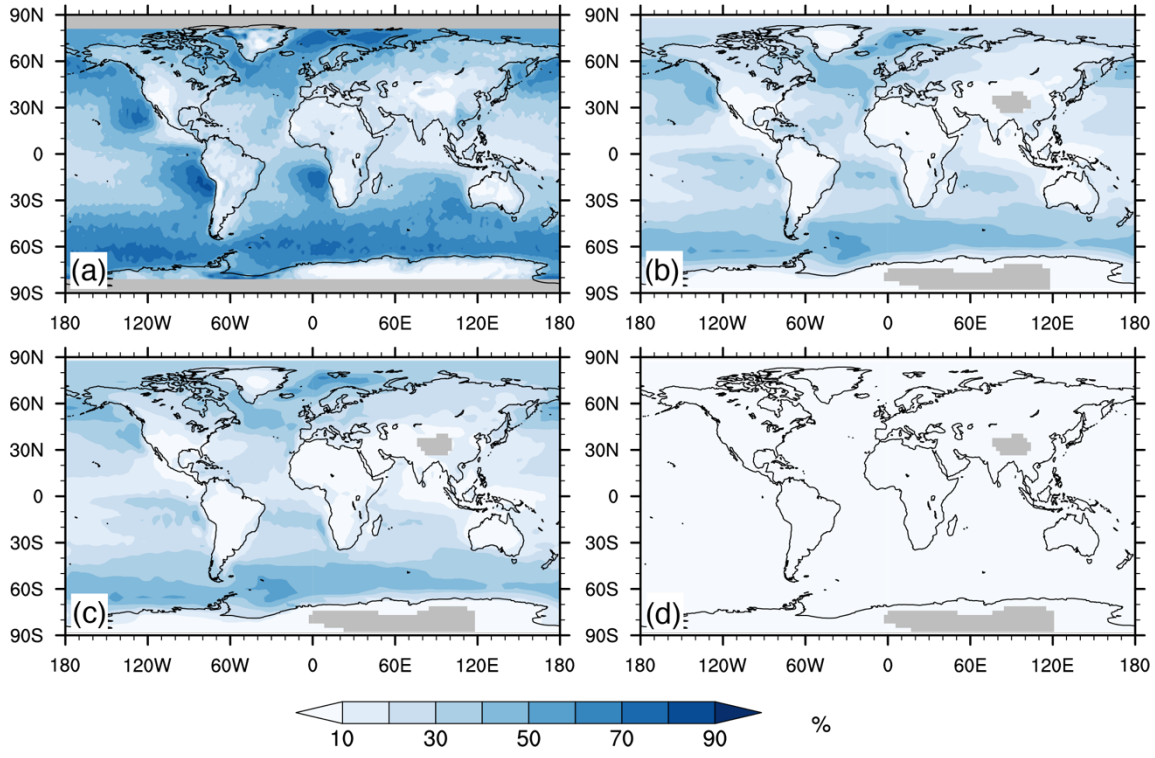

Figure A3: Annual mean low-level cloud cover (%): (a) CALIPSO-GOCCP (Chepfer et al., 2010); (b) PIvS; (c) PIvL; and (d) the difference between 1980-1999 in the historical and preindustrial simulations of Yoshimori et al. (2018). Note that low-level cloud cover is diagnosed assuming the maximum-random overlap for clouds with optical depth $\tau > 0.3$ as a standard model output.

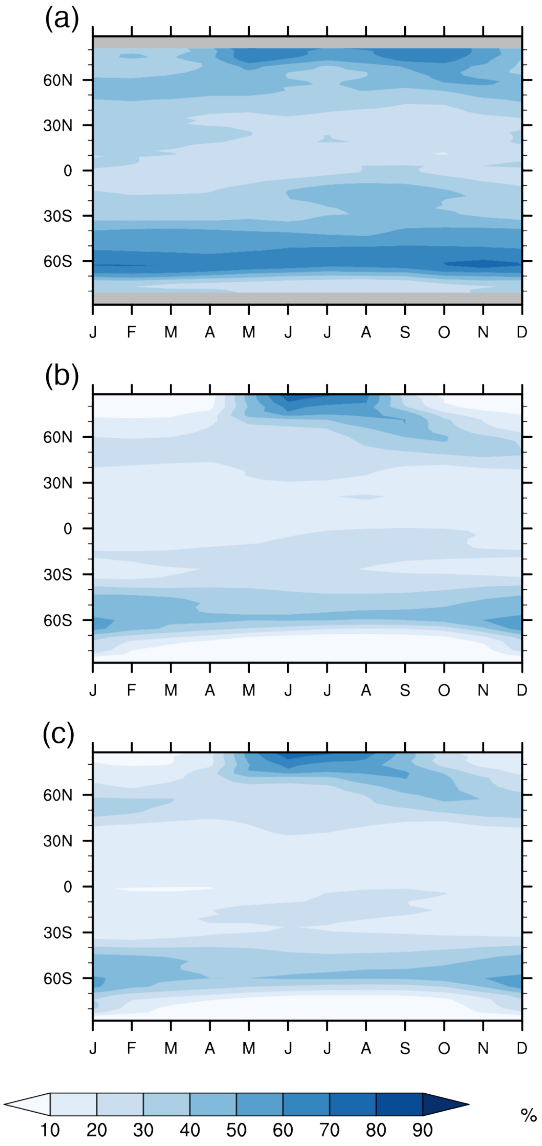

Figure A4: Seasonal progression of low-level cloud cover (%): (a) CALIPSO-GOCCP (Chepfer et al., 2010); (b) PIvS; and (c) PIvL. Note that low-level cloud cover is diagnosed assuming the maximum-random overlap for clouds with optical depth $\tau > 0.3$ as a standard model output.

Appendix B: AGCM experiment

As stated in the main text, we conducted sensitivity experiments using an AGCM component of the MIROC4m to isolate the effect of a perturbed cloud parameter (T_{ice} in Eq. 1) controlling the temperature-phase relationship from the effect of other perturbed cloud parameters (α and V_0 in Eqs. 2 and 3) controlling the autoconversion rate and ice sedimentation rate. The

influential parameter was identified by partially swapping these parameters. The list of experiments is presented in Table A1. An AGCM, instead of an AOGCM, was used to prevent the model from drifting away due to the Earth's energy imbalance. In Table A1, "Boundary conditions" refers to sea surface temperature, sea ice, and vegetation. Each AGCM experiment lasts 15 years, and the last 10 years were used for analysis.

We begin by examining the differences between the two cloud-parameter sets in PI simulations. Fig. A1a, which shows the differences in low-level cloud cover simulated by the AOGCM, is reproduced reasonably well in Fig. A1b, which shows the same field simulated with the AGCM. However, the experiment in which only T_{ice} is exchanged (Fig. A1c) fails to capture the main feature of the difference (cloud cover is reduced significantly instead of increasing), suggesting that the parameter T_{ice} plays a key role. On the other hand, the experiment in which α and V_0 are both exchanged (Fig. A1d) agrees with the sign of the complete response (Fig. A1b), suggesting that the result is qualitatively insensitive to these parameters. These results support our interpretation that the temperature-cloud phase relationship is the dominant factor in determining the difference between the two PI simulations of MIROC4mV.

Next, we focus on the difference between the two cloud-parameter sets in ΔLIG (LIG-PI). Fig. A2a, which shows the differences in low-level cloud cover simulated by the AOGCM, is reproduced reasonably well in Fig. A2b, which shows the same field simulated with the AGCM. Like the case of the difference in PI simulations, Fig. A2c fails to capture the main feature of the difference. Fig. A2d, on the other hand, agrees with the sign of the complete response (Fig. A2b). These results support our interpretation that the temperature-cloud phase relationship is the dominant factor in determining the difference between the two ΔLIG (difference of the difference) fields in MIROC4mV.

Table A1: A list of AGCM experiments

Experiments	Boundary conditions from MIROC4mV	Temperature dependency of cloud phase	Autoconversion and ice sedimentation
PIvS_SS	PIvS	S	S
PIvL_LL	PIvL	L	L
LIGvS_SS	LIGvS	S	S
LIGvL_LL	LIGvL	L	L
PIvS_LS	PIvS	L	S
PIvL_SL	PIvL	S	L
LIGvS_LS	LIGvS	L	S
LIGvL_SL	LIGvL	S	L
PIvS_SL	PIvS	S	L
PIvL_LS	PIvL	L	S
LIGvS_SL	LIGvS	S	L
LIGvL_LS	LIGvL	L	S

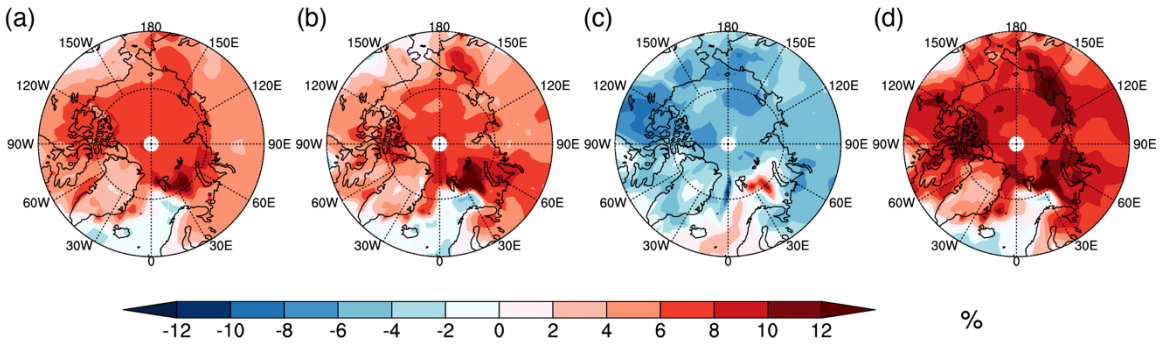

Figure A5: Difference in the annual mean low-level cloud cover (%): (a) PIvL – PIvS by MIROC4mV; (b) (a) reproduced by the AGCM (PIvL_LL – PIvS_SS); (c) AGCM with only the temperature-phase parameter swapped in (b) (PIvL_SL – PIvS_LS); and (d) AGCM with other cloud parameters swapped in (b) (PIvL_LS – PIvS_SL).

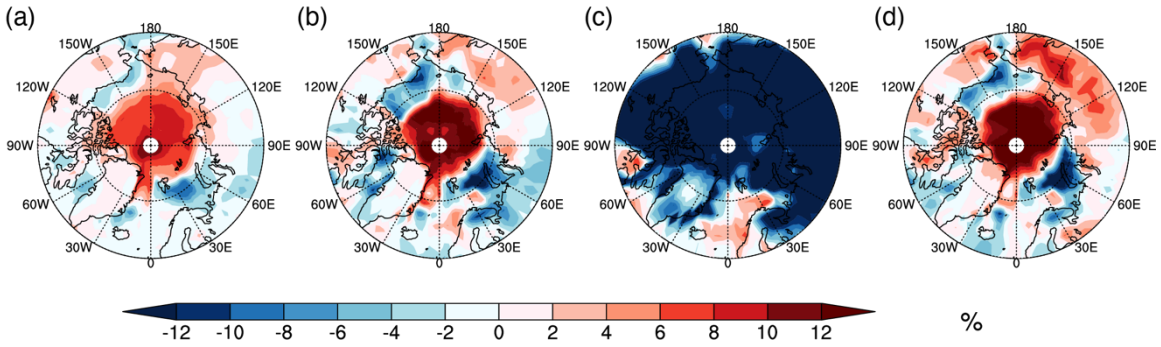

Figure A6: Difference in the October-December low-level cloud cover (%): (a) ΔLIGvL – ΔLIGvS by MIROC4mV; (b) (a) reproduced by the AGCM ([LIGvL_LL – LIGvS_SS] – [PIvL_LL – PIvS_SS]); (c) AGCM with only the temperature-phase parameter swapped in (b) ([LIGvL_SL – LIGvS_LS] –[PIvL_SL – PIvS_LS]); (d) AGCM with other cloud parameters swapped in (b) ([LIGvL_LS – LIGvS_SL] – [PIvL_LS – PIvS_SL]).

References

Abe, M., Nozawa, T., Ogura, T., and Takata, K.: Effect of retreating sea ice on Arctic cloud cover in simulated recent global warming, Atmospheric Chemistry and Physics, 16, 14343-14356, 2016.

Bartlein, P. J. and Shafer, S. L.: Paleo calendar-effect adjustments in time-slice and transient climate-model simulations (PaleoCalAdjust v1.0): impact and strategies for data analysis, Geoscientific Model Development, 12, 3889-3913, 2019.

Bennike, O., Bolshiyanov, D., Dowdeswell, J., Elverhoi, A., Geirsdottir, A., Hicks, S., Hubberton, H., Ingolfsson, O., Miller, G., and Members, C. P.: Holocene paleoclimate data from the Arctic: testing models of global climate change, Quaternary Science Reviews, 20, 1275-1287, 2001.

Box, J.E., R. Bellerby, R.E. Benestad, U.S. Bhatt, T.R. Christensen, C. Derksen, J. Francis, S. Gerland, K. Isaksen, J. Mård, J.L. McCarty, W.N. Meier, L. Mudryk, A. Shiklomanov, and S.L. Smith: Overview of multiple Arctic climate change indicators. In: AMAP Arctic Climate Change Update 2024: Key Trends and Impacts, pp. 5-12. Arctic Monitoring and Assessment Programme (AMAP), Tromsø, Norway, 2024.

CAPE: Last Interglacial Arctic warmth confirms polar amplification of climate change. Quat. Sci. Rev., 25, 1383-1400, 2006.

Capron, E., A. Govin, E. J. Stone, V. Masson-Delmotte, S. Mulitza, B. Otto-Bliesner, T. L. Rasmussen, L. C. Sime, C. Waelbroeck, and E. W. Wolff: Temporal and spatial structure of multi-millennial temperature changes at high latitudes during the Last Interglacial. Quat. Sci. Rev., 103, 116-133, 2014.

Capron, E., Govin, A., Feng, R., Otto-Bliesner, B. L., and Wolff, E. W.: Critical evaluation of climate syntheses to benchmark CMIP6/PMIP4 127 ka Last Interglacial simulations in the high-latitude regions, Quaternary Science Reviews, 168, 137-150, 2017.

Chan, W.-L. and Abe-Ouchi, A.: Pliocene Model Intercomparison Project (PlioMIP2) simulations using the Model for Interdisciplinary Research on Climate (MIROC4m), Climate of the Past, 16, 1523-1545, 2020.

Chepfer, H., S. Bony, D. Winker, G. Cesana, J. L. Dufresne, P. Minnis, C. J. Stubenrauch, and S. Zeng: The GCM-Oriented CALIPSO Cloud Product (CALIPSO-GOCCP). J. Geophys. Res., 115, D00H16, 2010. https://doi.org/10.1029/2009JD012251.

Cline, R. M. L., J. D. Hays, W. L. Prell, W. F. Ruddiman, T. C. Moore, N. G. Kipp, B. E. Molfino, G. H. Denton, T. J. Hughes, W. L. Balsam, C. A. Brunner, J.-C. Duplessy, A. G. Esmay, J. L. Fastook, J. Imbrie, L. D. Keigwin, T. B. Kellogg, A. McIntyre, R. K. Matthews, A. C. Mix, J. J. Morley, N. J. Shackleton, S. S. Streeter, and P. R. Thompson: The Last Interglacial Ocean. Quaternary Research, 21, 123-224, 2017.

Diamond, R., Sime, L. C., Schroeder, D., and Guarino, M.-V.: The contribution of melt ponds to enhanced Arctic sea-ice melt during the Last Interglacial, The Cryosphere, 15, 5099-5114, 2021.

Diamond, R., D. Schroeder, L. C. Sime, J. Ridley, D. Feltham: The significance of the melt-pond scheme in a CMIP6 global climate model. J. Climate, 37, 249–268, 2024.

Guarino, M.-V., L. C. Sime, D. Schroeder, I. Malmierca-Vallet, E. Rosenblum, M. Ringer, J. Ridley, D. Feltham, C. Bitz, E. Steig, E. Wolff, J. Stroeve, and A. Sellar: Sea-ice-free Arctic during the Last Interglacial supports fast future loss. Nature Clim. Chan., 10, 928-932, 2020.

Guarino, M. V. and L. C. Sime: Last Interglacial summer air temperature observations for the Arctic (Version 1.0) [Data set]. NERC EDS UK Polar Data Centre. https://doi.org/10.5285/9AB58D27-596A-472C-A13E-2DCD68612082, 2022.

Gulev, S. K., Thorne, P. W., Ahn, J., Dentener, F. J., Domingues, C. M., Gerland, S., Gong, D., Kaufman, D. S., Nnamchi, H. C., Quaas, J., Rivera, J. A., Sathyendranath, S., Smith, S. L., Trewin, B., Schuckmann, K. v., and Vose, R. S.: Changing State of the Climate System. In: Climate Change 2021: The Physical Science Basis., Masson-Delmotte, V., P. Zhai, A. Pirani, S.L. Connors, C. Péan, S. Berger, N. Caud, Y. Chen, L. Goldfarb, M.I. Gomis, M. Huang, K. Leitzell, E. Lonnoy, and J.B.R. Matthews, T. K. M., T. Waterfield, O. Yelekçi, R. Yu, and B. Zhou (Eds.), Cambridge University Press, Cambridge, United Kingdom and New York, NY, USA, 2021.

Hersbach, H., Bell, B., Berrisford, P., Hirahara, S., Horányi, A., Muñoz-Sabater, J., Nicolas, J., Peubey, C., Radu, R., Schepers, D., Simmons, A., Soci, C., Abdalla, S., Abellan, X., Balsamo, G., Bechtold, P., Biavati, G., Bidlot, J., Bonavita, M., De Chiara, G., Dahlgren, P., Dee, D., Diamantakis, M., Dragani, R., Flemming, J., Forbes, R., Fuentes, M., Geer, A., Haimberger, L., Healy, S., Hogan, R. J., Hólm, E., Janisková, M., Keeley, S., Laloyaux, P., Lopez, P., Lupu, C., Radnoti, G., de Rosnay, P., Rozum, I., Vamborg, F., Villaume, S., and Thépaut, J. N.: The ERA5 global reanalysis, Quarterly Journal of the Royal Meteorological Society, 146, 1999-2049, 2020.

Hirose, L. A., Abe-Ouchi, A., Chan, W. L., O'Ishi, R., Yoshimori, M., and Obase, T.: Arctic Warming Suppressed by Remnant Glacial Ice Sheets in Past Interglacials, Geophysical Research Letters, 52, 2025.

K-1 model developers, X.: K-1 coupled model (miroc) description, Tech. rep., Center for Climate System Research, The University of Tokyo, 2004. 2004.

Kageyama, M., Sime, L. C., Sicard, M., Guarino, M.-V., de Vernal, A., Stein, R., Schroeder, D., Malmierca-Vallet, I., Abe-Ouchi, A., Bitz, C., Braconnot, P., Brady, E. C., Cao, J., Chamberlain, M. A., Feltham, D., Guo, C., LeGrande, A. N., Lohmann, G., Meissner, K. J., Menviel, L., Morozova, P., Nisancioglu, K. H., Otto-Bliesner, B. L., O'Ishi, R., Ramos Buarque, S., Salas y Melia, D., Sherriff-Tadano, S., Stroeve, J., Shi, X., Sun, B., Tomas, R. A., Volodin, E., Yeung, N. K. H., Zhang, Q., Zhang, Z., Zheng, W., and Ziehn, T.: A multi-model CMIP6-PMIP4 study of Arctic sea ice at 127 ka: sea ice data compilation and model differences, Climate of the Past, 17, 37-62, 2021.

Kay, J. E., L'Ecuyer, T., Chepfer, H., Loeb, N., Morrison, A., and Cesana, G.: Recent Advances in Arctic Cloud and Climate Research, Current Climate Change Reports, 2, 159-169, 2016.

Keen, A., Blockley, E., Bailey, D. A., Boldingh Debernard, J., Bushuk, M., Delhaye, S., Docquier, D., Feltham, D., Massonnet, F., O'Farrell, S., Ponsoni, L., Rodriguez, J. M., Schroeder, D., Swart, N., Toyoda, T., Tsujino, H., Vancoppenolle, M., and Wyser, K.: An inter-comparison of the mass budget of the Arctic sea ice in CMIP6 models, The Cryosphere, 15, 951–982, 2021.

Kuniyoshi, Y., Abe-Ouchi, A., Sherriff-Tadano, S., Chan, W. L., and Saito, F.: Effect of Climatic Precession on Dansgaard-Oeschger-Like Oscillations, Geophysical Research Letters, 49, 2022.

Lu, J. H. and Cai, M.: Seasonality of polar surface warming amplification in climate simulations, Geophysical Research Letters, 36, 2009.

Malmierca-Vallet, I. L. C. Sime, J. C. Tindall, E. Capron, P. J. Valdes, B. M. Vinther, and M. D. Holloway: Simulating the Last Interglacial Greenland stable water isotope peak: The role of Arctic sea ice changes. Quat. Sci. Rev., 198, 1-14, 2018.

McCoy, D. T., Hartmann, D. L., Zelinka, M. D., Ceppi, P., and Grosvenor, D. P.: Mixed-phase cloud physics and Southern Ocean cloud feedback in climate models, Journal of Geophysical Research-Atmospheres, 120, 9539-9554, 2015.

McKay, N. P., J. T. Overpeck, and B. L. Otto-Bliesner: The role of ocean thermal expansion in Last Interglacial sea level rise. Geophys. Res. Lett., 38, L14605, doi:10.1029/2011GL048280, 2011.

Morrison, H., de Boer, G., Feingold, G., Harrington, J., Shupe, M. D., and Sulia, K.: Resilience of persistent Arctic mixed-phase clouds, Nature Geoscience, 5, 11-17, 2011.

Murray, B. J., Carslaw, K. S., and Field, P. R.: Opinion: Cloud-phase climate feedback and the importance of ice-nucleating particles, Atmospheric Chemistry and Physics, 21, 665-679, 2021.

O'ishi, R., Abe-Ouchi, A., Prentice, I. C., and Sitch, S.: Vegetation dynamics and plant CO2responses as positive feedbacks in a greenhouse world, Geophysical Research Letters, 36, 2009.

O'ishi, R., Chan, W.-L., Abe-Ouchi, A., Sherriff-Tadano, S., Ohgaito, R., and Yoshimori, M.: PMIP4/CMIP6 last interglacial simulations using three different versions of MIROC: importance of vegetation, Climate of the Past, 17, 21-36, 2021.

Ogura, T., Emori, S., Webb, M. J., Tsushima, Y., Yokohata, T., Abe-Ouchi, A., and Kimoto, M.: Towards understanding cloud response in atmospheric GCMs: The use of tendency diagnostics, Journal of the Meteorological Society of Japan, 86, 69-79, 2008.

Otto-Bliesner, B. L., Braconnot, P., Harrison, S. P., Lunt, D. J., Abe-Ouchi, A., Albani, S., Bartlein, P. J., Capron, E., Carlson, A. E., Dutton, A., Fischer, H., Goelzer, H., Govin, A., Haywood, A., Joos, F., LeGrande, A. N., Lipscomb, W. H., Lohmann, G., Mahowald, N., Nehrbass-Ahles, C., Pausata, F. S. R., Peterschmitt, J.-Y., Phipps, S. J., Renssen, H., and Zhang, Q.: The PMIP4 contribution to CMIP6 – Part 2: Two interglacials, scientific objective and experimental design for Holocene and Last Interglacial simulations, Geoscientific Model Development, 10, 3979-4003, 2017.

Otto-Bliesner, B. L., Brady, E. C., Zhao, A., Brierley, C. M., Axford, Y., Capron, E., Govin, A., Hoffman, J. S., Isaacs, E., Kageyama, M., Scussolini, P., Tzedakis, P. C., Williams, C. J. R., Wolff, E., Abe-Ouchi, A., Braconnot, P., Ramos Buarque, S., Cao, J., de Vernal, A., Guarino, M. V., Guo, C., LeGrande, A. N., Lohmann, G., Meissner, K. J., Menviel, L., Morozova, P. A., Nisancioglu, K. H., O'Ishi, R., Salas y Mélia, D., Shi, X., Sicard, M., Sime, L., Stepanek, C., Tomas, R., Volodin, E., Yeung, N. K. H., Zhang, Q., Zhang, Z., and Zheng, W.: Large-scale features of Last Interglacial climate: results from evaluating the <i>lig127k</i> simulations for the Coupled Model Intercomparison Project (CMIP6)–Paleoclimate Modeling Intercomparison Project (PMIP4), Climate of the Past, 17, 63-94, 2021.

Past Interglacials Working Group of PAGES: Interglacials of the last 800,000 years. Reviews of Geophysics, 54, 162-219, 2016.

Rantanen, M., A. Y. Karpechko, A. Lipponen, K. Nordling, O. Hyvärinen, K. Ruosteenoja, T. Vihma, and A. Laaksonen: The Arctic has warmed nearly four times faster than the globe since 1979. Commun. Earth Environ., 3, 168, doi:10.1038/s43247-022-00498-3, 2022.

Razmjooei, M. J., J. Henderiks, H. K. Coxall, K.-H. Baumann, F. Vermassen, M. Jakobsson, F. Niessen, and M. O'Regan: Revision of the Quaternary calcareous nannofossil biochronology of Arctic Ocean sediments, Quat. Sci. Rev., 321, 108 3846, 2023.

Sagoo, N., Storelvmo, T., Hahn, L., Tan, I., Danco, J., Raney, B., and Broccoli, A. J.: Observationally Constrained Cloud Phase Unmasks Orbitally Driven Climate Feedbacks, Geophysical Research Letters, 48, 2021.

Screen, J. A., and I. Simmonds: The central role of diminishing sea ice in recent Arctic temperature amplification. Nature, 464, 1334–1337, 2010.

Sherriff-Tadano, S., Abe-Ouchi, A., Yoshimori, M., Ohgaito, R., Vadsaria, T., Chan, W. L., Hotta, H., Kikuchi, M., Kodama, T., Oka, A., and Suzukia, K.: Southern Ocean Surface Temperatures and Cloud Biases in Climate Models Connected to the Representation of Glacial Deep Ocean Circulation, Journal of Climate, 36, 3849-3866, 2023.

Sicard, M., M. Kageyama, S. Charbit, P. Braconnot, and J.-B. Madeleine, 2022: An energy budget approach to understand the Arctic warming during the Last Interglacial. Climate Past, 18, 607–629.

Sime, L. C., R. Sivankutty, I. Malmierca-Vallet, A. M. de Boer, and M. Sicard: Summer surface air temperature proxies point to near-sea-ice-free conditions in the Arctic at 127 ka. Clim. Past, 19, 883-900, 2023.

Sime, L. C., R. Diamond, C. Stepanek, C. Brierley, D. Schroeder, M. Kageyama, I. Malmierca-Vallet, E. Blockley, A. West, D. Feltham, J. Ridley, P. Braconnot, C. J. R. Williams, X. Shi, B. L. Otto-Bliesner, S. I. Macarewich, S. R. Buarque, Q. Zhang, A. LeGrande, W. Zheng, D. Jiang, P. Morozova, C. Guo, Z. Zhang, N. Yeung, L. Menviel, S. Narayanasetti, O. Reeves, M. Pollock, and A. Zho: A sea ice free Arctic: Assessment Fast Track abrupt-127k experimental protocol and mnotivation. EGU sphere Discussion, https://doi.org/105194/egusphere-2025-3531, 2025.

Sitch, S., Smith, B., Prentice, I. C., Arneth, A., Bondeau, A., Cramer, W., Kaplan, J. O., Levis, S., Lucht, W., Sykes, M. T., Thonicke, K., and Venevsky, S.: Evaluation of ecosystem dynamics, plant geography and terrestrial carbon cycling in the LPJ dynamic global vegetation model, Global Change Biology, 9, 161-185, 2003.

Slivinski, L. C., Compo, G. P., Sardeshmukh, P. D., Whitaker, J. S., McColl, C., Allan, R. J., Brohan, P., Yin, X., Smith, C. A., Spencer, L. J., Vose, R. S., Rohrer, M., Conroy, R. P., Schuster, D. C., Kennedy, J. J., Ashcroft, L., Brönnimann, S.,

Brunet, M., Camuffo, D., Cornes, R., Cram, T. A., Domínguez-Castro, F., Freeman, J. E., Gergis, J., Hawkins, E., Jones, P. D., Kubota, H., Lee, T. C., Lorrey, A. M., Luterbacher, J., Mock, C. J., Przybylak, R. K., Pudmenzky, C., Slonosky, V. C., Tinz, B., Trewin, B., Wang, X. L., Wilkinson, C., Wood, K., and Wyszyński, P.: An Evaluation of the Performance of the Twentieth Century Reanalysis Version 3, Journal of Climate, 34, 1417-1438, 2021.

Tan, I. and Storelvmo, T.: Evidence of Strong Contributions From Mixed-Phase Clouds to Arctic Climate Change, Geophysical Research Letters, 46, 2894-2902, 2019.

Tan, I., Storelvmo, T., and Zelinka, M. D.: Observational constraints on mixed-phase clouds imply higher climate sensitivity, Science, 352, 224-227, 2016.

Tan, I., C. Zhou, A. Lamy, and C. L. Stauffer: Moderate climate sensitivity due to opposing mixed-phase cloud feedbacks, npj Climate and Atmospheric Science, 8, 86, 2025. https://doi.org/10.1038/s41612-025-00948-7.

Titchner, H. A., and N. A. Rayner: The Met Office Hadley Centre sea ice and sea surface temperature data set, version 2: 1. Sea ice concentrations, J. Geophys. Res. Atmos., 119, 2864-2889, 2014. doi: 10.1002/2013JD020316.

Tsushima, Y., Emori, S., Ogura, T., Kimoto, M., Webb, M. J., Williams, K. D., Ringer, M. A., Soden, B. J., Li, B., and Andronova, N.: Importance of the mixed-phase cloud distribution in the control climate for assessing the response of clouds to carbon dioxide increase: a multi-model study, Climate Dynamics, 27, 113-126, 2006.

Turney, C. S. M. and Jones, R. T.: Does the Agulhas Current amplify global temperatures during super-interglacials?, Journal of Quaternary Science, 25, 839-843, 2010.

Turney, C. S. M., R. T. Jones, N. P. McKay, E. van Sebille, Z. A. Thomas, C.-D. Hillenbrand, and C. J. Fogwill: A global mean sea surface temperature dataset for the Last Interglacial (129–116 ka) and contribution of thermal expansion to sea level change. Earth Syst. Sci. Data, 12, 3341-3356, 2020.

Vermassen, F., O'Regan, M., de Boer, A., Schenk, F., Razmjooei, M., West, G., Cronin, T. M., Jakobsson, M., and Coxall, H. K.: A seasonally ice-free Arctic Ocean during the Last Interglacial, Nature Geoscience, 2023. doi: 10.1038/s41561-023-01227-x, 2023.

Yoshimori, M., A. Abe-Ouchi, H. Tatebe, T. Nozawa, and A. Oka: The importance of ocean dynamical feedback for understanding the impact of mid-high-latitude warming on tropical precipitation change. J. Climate, 31, 2417-2434, 2018.

Yoshimori, M., Kawasaki, T., Abe-Ouchi, A., and Hasumi, H.: Arctic Amplification in the Past, Present, and Future: A Review for the Challenge to the Integrative Understanding of its Mechanism, Journal of the Meteorological Society of Japan, 103, 523-558, 2025.

Yoshimori, M., Yokohata, T., and Abe-Ouchi, A.: A Comparison of Climate Feedback Strength between CO_2 Doubling and LGM Experiments, Journal of Climate, 22, 3374-3395, 2009.

Zelinka, M. D., Myers, T. A., McCoy, D. T., Po-Chedley, S., Caldwell, P. M., Ceppi, P., Klein, S. A., and Taylor, K. E.: Causes of Higher Climate Sensitivity in CMIP6 Models, Geophysical Research Letters, 47, 2020.